Title

Structural Evaluation of Hybrid Low-Density Polyethylene (LDPE)/ Fiber Reinforced Polymer (FRP) Composite Collision Protective System for Highway Bridges

Permalink

Author

Doddawadamath, Swaroop Shivanand

Publication Date

2016

Peer reviewed|Thesis/dissertation

UNIVERSITY OF CALIFORNIA, IRVINE

Structural Evaluation of Hybrid Recycled Low-Density Polyethylene (LDPE)/ Fiber Reinforced Polymer (FRP) Composite Collision Protective System for Highway Bridges

THESIS

submitted in partial satisfaction of the requirements for the degree of

MASTER OF SCIENCE

In Civil Engineering

by

Swaroop Shivanand Doddawadamath

Thesis Committee:
Professor Ayman S Mosallam, Chair
Professor Mohammad Javad Abdolhosseini Qomi
Professor Farghalli A Mohamed

2016

DEDICATION

To my parents and friends for their unconditional love

and continuous support throughout my life

TABLE OF CONTENTS

LIST OF FIGURES

LIST OF TABLES

ACKNOWLEDGMENTS

ABSTRACT OF THE THESIS

Structural Evaluation of Hybrid Recycled Low Density Polyethylene (LDPE)/ Fiber Reinforced Plastic (FRP) Composite Collision Protective System for Highway Bridges

By

Swaroop Shivanand Doddawadamath

Master of Science in Civil and Environmental Engineering

University of California, Irvine, 2016

Professor Ayman Mosallam, Chair

The thesis focuses on a research study that included the experimental, analytical and finite element modeling of structural evaluation of hybrid LDPE/FRP composite beams. Two FRP composite reinforcement details were evaluated in this investigation. In addition, results of axial tensile and compression coupon tests to characterize the short-term mechanical properties of LDPE/FRP matrix are presented and discussed. The experimental results of two large-scale hybrid beam specimens subjected to quasi-static four-point loading, that were performed by Mosallam (2005), are discussed. Results obtained from the experimental tests showed that due to the hybrid nature of the beam specimens and the viscoelastic/elastoplastic behavior of the LDPE matrix, flexural stiffness of the two beams were dependent on the stress level as well as on the loading rate. The change in the stiffness can also be attributed to the initial cyclic loading that was performed up to 10.0 kips (44.5 kN) which typically will result in a slight permanent set similar to the typical behavior of other materials such as reinforced concrete members. Due to the absence of

ASTM standards or Caltrans (California Department of Transportation) procedures for determining experimentally the flexural stiffness of such hybrid beams, a simple procedure was used to calculate the flexural stiffness of the hybrid beams at different loading levels. In general, the load-deflection behavior of the beam specimen was linear up to about 80% of the ultimate load, after which the behavior became and continued to be non-linear up to the ultimate load. Based on visual inspection, no local damages or cracks were observed in the LDPE matrix, and the governing mode of failure was in the form of resulted relative slippage of the FRP rebars and the LDPE matrix at beam ends, especially the top compressive reinforcements that resulted in stiffness degradation. This is can be attributed to the thermo-mechanical mismatch between the matrix and the reinforcing materials. Due to the relatively low flexural stiffness of the tested hybrid beams, the maximum load for the tests was limited by the maximum hydraulic actuator stroke. An analytical model that was developed by Mosallam (2005) is described and verified with the experimental results. In addition, finite element models were developed for different beam geometries and reinforcement details. Several runs were performed and numerical results were analyzed and discussed. Conclusions and recommendations for future research related to this area are also presented.

CHAPTER 1

INTRODUCTION

1.1. OVERVIEW

This thesis summarizes the comparison of experimental, analytical and finite element modeling results of two beam specimens that were tested under quasi-static loading/unloading and loading-to-failure protocol. The degradation and deterioration of the conventional building materials like timber, concrete and steel piling system (Figure 1.1) led to the birth of alternative construction material such as Fiber Reinforced Polymer (FRP) composites without the performance disadvantages of traditional materials. The FRP reinforcements was selected to alienate the potential of corrosion that typically occurs to steel reinforcement especially in wet environments.

Figure (1.1): Deterioration of conventional timber and concrete piles

The use of recycled plastics and polymer products has a potential positive impact on both the environment as well as world energy consumption. In past decade or so, a global movement on protecting earth environment and conserving energy has been initiated. Based on the information published by the US Department of Energy and other

international organizations, it is evident that the large portion of the energy consumption and environmental damages are related to construction sector including materials, processes and built environment. Recycling waste polymeric materials such as plastic bags, plastic bottles and including these materials as major components of to any construction materials will have a major positive impact on both environment and energy conservation.

In the last few years, several initiatives on using construction materials that are made in part from waste plastics have been reported. For example, plastic lumber products for non-structural applications such as flooring, children playground structures were introduced in early 1990. Primary and secondary structural systems for marine and harbor applications such as plastic piles, marine fenders and camels were offered by several companies in the USA. Several marine applications using recycled hybrid systems were constructed as demonstration projects by the US Army Corps, US Navy, port authorities in USA (*e.g. Port Wanimaie, Delaware Port Authority, etc.*) and recently, California Department of Transportation (Caltrans). Figures (1.2 through 1.4) show examples of LDPE systems in marine applications. Caltrans introduced a new structural application for highway bridges where recycled LDPE/FRP hybrid beams (*or camels*) are used as a protection system for highway bridge abutments from potential impact by ships and barges. This paper provides results of a pilot experimental and analytical investigation on the flexural performance of LDPE/FRP composite beams with different reinforcement arrangements under service and ultimate quasi-static loads.

Figure (1.2): Fender piles in the U.S. Naval Submarine Base, San Diego, CA

Figure (1.3): Fendering system in the U.S. Navy Pier 10, San Diego, CA

Figure (1.4): Fendering system, Nashville Avenue Marine Terminal
Port of New Orleans, LA, USA

1.2. RESEARCH OBJECTIVES

The main objectives of this research study are:

1. Analysis of large-scale experimental results conducted on hybrid LDPE/FRP composite beams with different details,

2. Review, description and verification of Mosallam (2008) analytical model for hybrid LDPE/FRP composite flexural members

3. Numerical simulation of the quasi-static behaviour of hybrid LDPE/FRP composite beams.

4. Comparison and correlation between experimental and analytical results,

5. Drawing conclusions on behaviour and feasibility of using such hybrid system in different bridge applications, and

6. Identification and recommendations of areas of future research related to LDPE hybrid beams recommendations for future research.

1.3. LITERATURE REVIEW

An experimental investigation of the structural behavior of HDPE pile was conducted by Asaro (2010). The objectives of the three point bend tests performed were to determine the flexural stiffness of the piling, the maximum point load up to failure (Figure 1.5). Hybrid Steel/HDPE Piling mode of failure of the piling. Specifically, it was of interest to document whether the piling would fail in a ductile manner, thus absorbing large amounts of energy, or by a more catastrophic manner, thus absorbing relatively small amounts of energy.The result showed permanent deformation, along with the effect of the point loading in causing localized deformation. No cracking or spalling was observed during and after the test even after full yielding. A test on tensile and bond properties of Glass Fiber Reinforced Plastic rebars(GFRP) was performed by Malvar (1995) to analyze the surface deformations experimentally. A detailed paper focusing on behavior of the interface between rebar and concrete was published. The tensile tests using FRP rebar specimens instead of coupons showed deep indentations and the resulting kinks in the longitudinal fibers will reduce bar strength. In 2010, another research study was conducted by Iskander at New York Polytechnic Institute on degradation and durability on FRP composite piles (see Figure 1.6). A set of conclusions were derived on durability, environmental factors, cost, long-term records that concluded that the use of such system is suitable for marine applications..
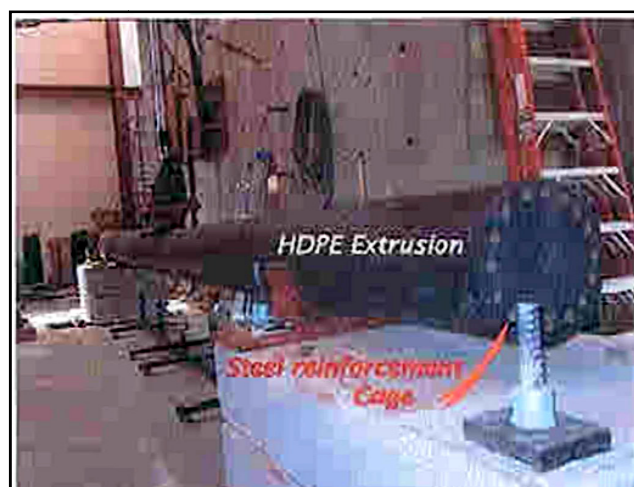
Figure (1.5): Three point bend test (Asaro, 2010)
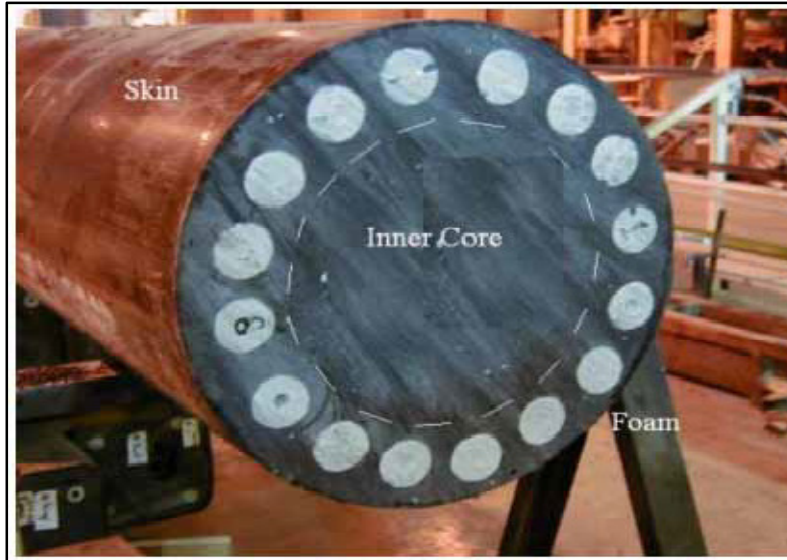
Figure (1.6): Typical HDPE/LDPE steel reinforcement composite pile (Asaro, 2010)

Several experiments were carried out against dynamic loading and its effects on barge collision with a bridge pier. A nonlinearlaboratory tests and numerical analysis of barge collision with a single bridge pier was performed by Yan and Sha (2012). An elastic-plastic model was employed with concrete column with steel reinforcement. To investigate the effects of reinforced concrete pier deformationand damage on barge–pier collision, detailed nonlinear concrete and steel material properties are considered in modeling the bridge pier. Retrofitting, repair and rehabilitation of reinforced concrete members using FRP composites is reported by Mosallam AS (2014). The paper focuses on all composite structural applications that include bridges and buildings and also the development of latest design codes, material specifications and international standards for composites in civil infrastructure applications.

Some of the tests on the mechanical properties such as durability and long term performance of High-Density Polyethylene (HDPE) and Low-Density Polyethylene (LDPE) has been described by Arnepalli and Rejoice (2012). Other properties such as Poisson's ratio and mechanical non linearity under tensile deformation of HDPE and LDPE have been discussed by Nitta and Yamana (2012). All the above information has been the backbone in developing the idea of this project and report.

1.3.1 HYBRID LDPE COMPOSITE BEAM

Plastics are divided into two basic groups, thermoplastics and thermosets, both of which are used to produce plastic pipe. Thermoplastics include compositions of polyethylene, polypropylene, polybutylene and PVC. Thermoset plastics are similar to thermoplastics prior to "curing", a chemical reaction by which polymer chains are chemically bonded to each other by new cross-links. E-glass/polyester is the most popular reinforcement and e-glass/polyester-reinforced pipe (FRP) is the most common for producing thermoset-type pipes. Side branching is the random bonding of short polymer chains to the main polymer chain. Since branched chains are unable to pack together very tightly, the resulting material is a relatively low density, which led to it being named low-density polyethylene (LDPE). As depicted in Figure 1.7, the stress/strain response for polyethylene is profoundly dependent on the tensile test conditions.
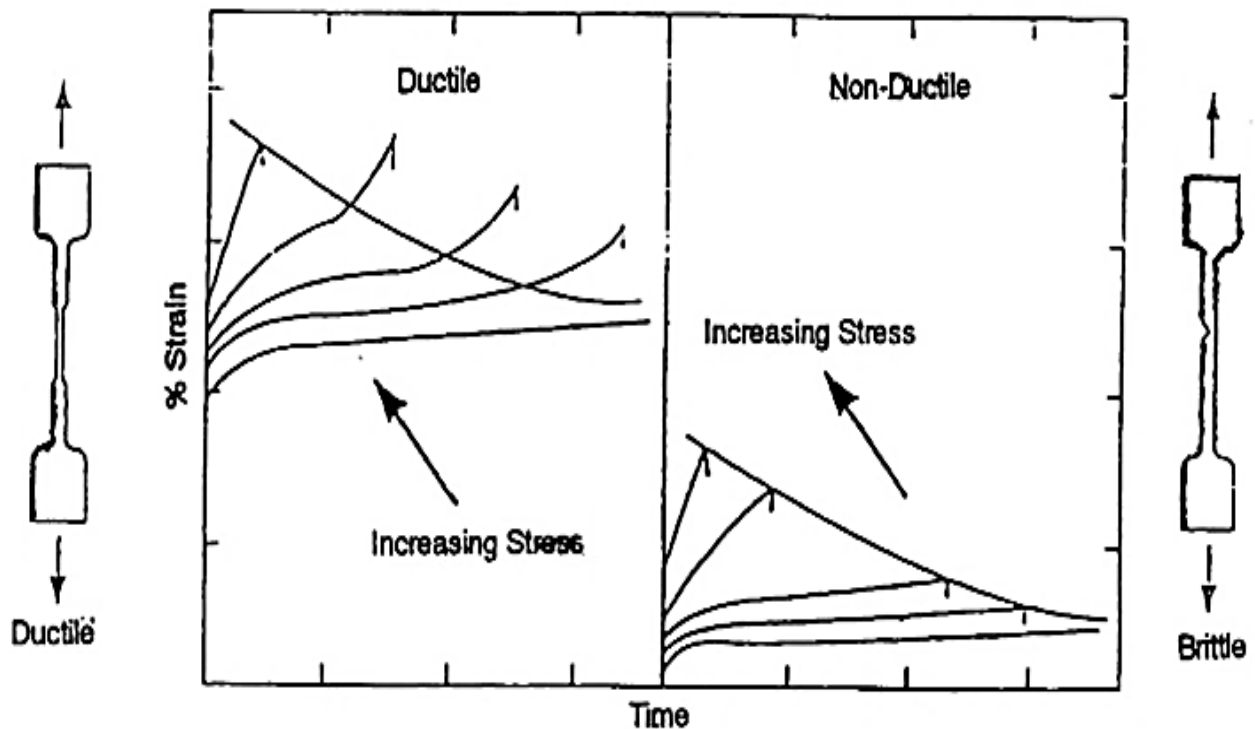
Figure (1.7): Stress-Strain relationship with respect to time for polyethylene

1.3.2 FIBER-REINFORCED-POLYMER (FRP) COMPOSITE REBARS

The experimental work described herein includes laboratory tests on the mechanical behavior, flexural behavior, and buckling resistance of FRP pile materials. The E-glass/polyester rebars are manufactured in a pultrusion process, using E-glass/polyester strands and polyester resin. Recycled plastic is composed mainly of high(HDPE), medium (MDPE) and low- density polypropylene (LDPE). Typical stress-strain curves for FRP composites rebars is presented in (Figure 1.8). Relative to steel and carbon fiber composites (CFRP), glass fiber composites (GFRP) have low stiffness which is advantageous in fendering application.
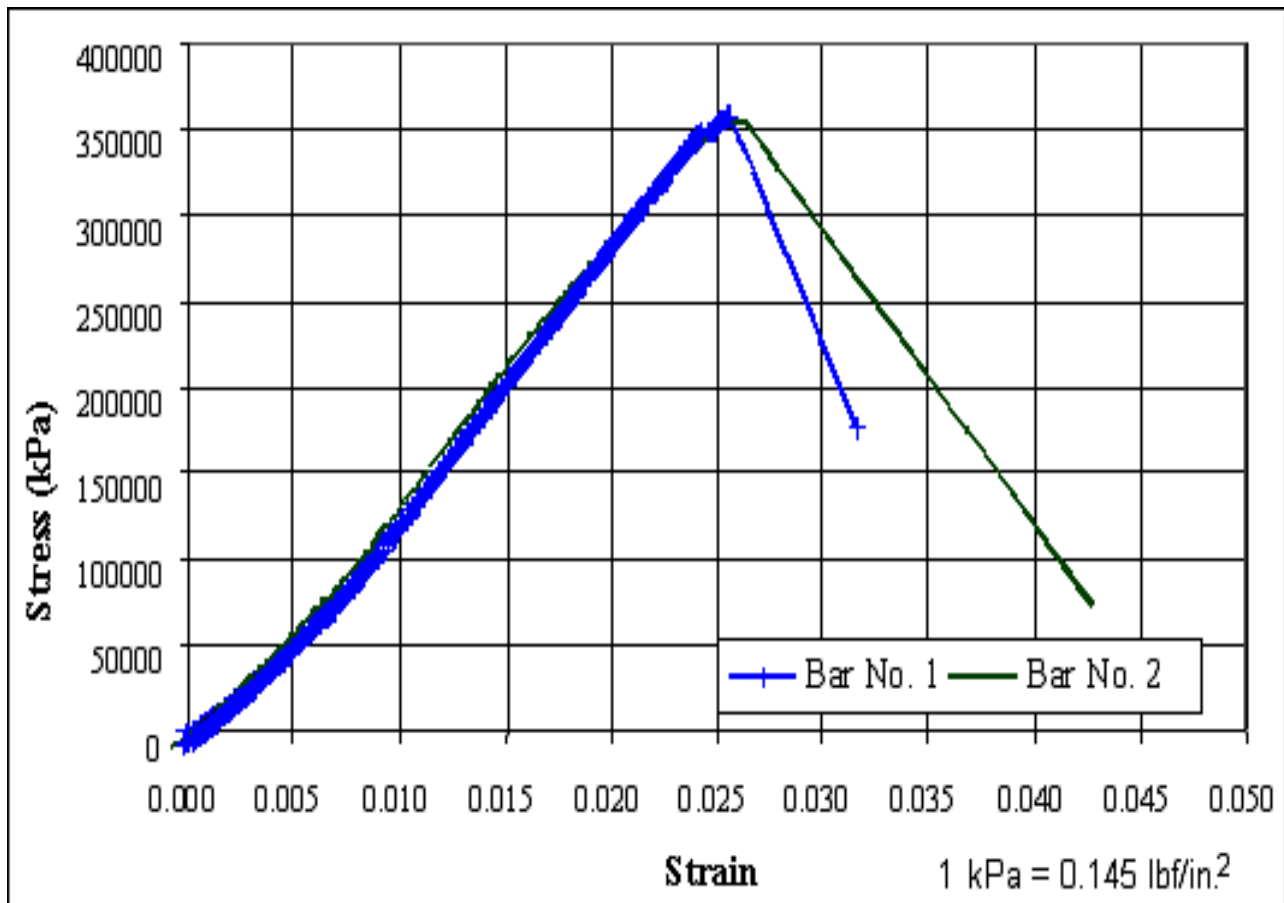
Figure (1.8): Stress-Strain relationship in E-glass/polyester rebars

CHAPTER 2

EXPERIMENTAL EVALUATION OF LDPE-FRP HYBRID BEAMS

2.1 GENERAL

In this chapter, a description of the experimental program conducted at UCI (Mosallam, 2005) regarding the dimensions and specifications of specimen, material properties, structural evaluation, test setup, loading patterns, failure modes and other results are presented. Two types of tests are described in this chapter: (i) matrix and reinforcement materials characterization coupon tests, and (ii) large-scale 4-point loading/unloading beam tests.

2.2 COUPON TESTS

Several LDPE coupon specimens were tested under both tension and compression using a calibrated INSTRON1125 and 3367 testing machines. Three different types of specimen were cut for tensile and compressive testing (Figures 2.1 and 2.2). Tensile specimen were cut in the cylindrical space with grip on each side for testing on the Instron 1125 machine. The compressive specimens were cut in cylindrical shape with short gauge length with no grip on either side and tested on Instron 3367 and also Instron 1125 (refer to Figures 2.3 and 2.4).

(a)   *(b)*
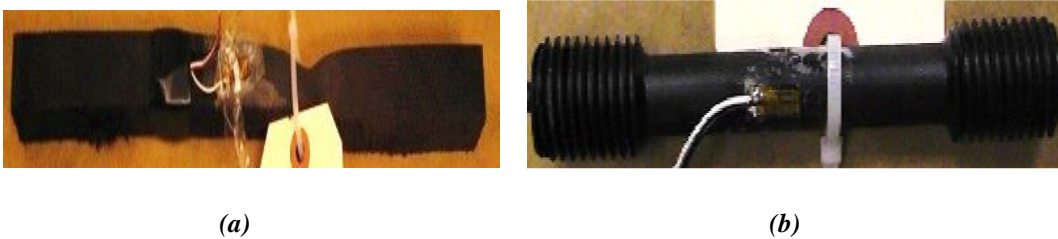
Figure (2.1): LDPE Specimens for: (a) tensile tests and (b) compressive tests
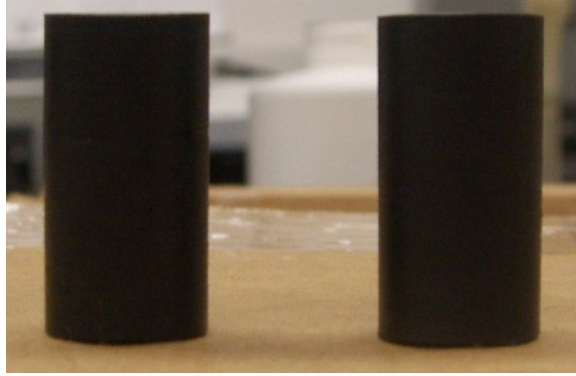
Figure (2.2): Specimen prepared for compressive testing
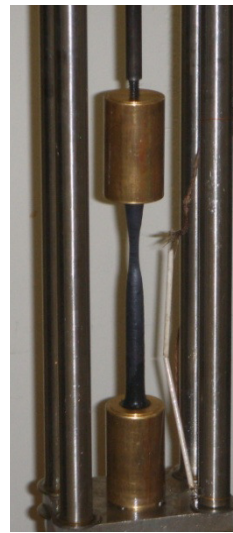
Figure (2.3): Specimen Tensile testing in Instron 1125

The specimen yielded before the rupture occurred [Mosallam 2005]

Figure (2.4): Specimen Tensile testing in Instron 3367

The specimen is starting to yield. The deformation observed up to 300%.

The first two tensile tests were performed on Instron1125 electro-mechanical testing machine. The results obtained from the Instron 1125 are plotted on graph paper in a load vs. time format. Using the results, one can convert the load and time into stress and strain. During the first tensile test, the test was stopped after 2.5 hours because the strain rate was too slow. The maximum load recorded was 1.35 ksi (9.3 MPa) and the strain was around 21%. Thus, the tensile test was repeated again on the same machine with faster strain rate and the observed maximum stress was 2.91 ksi (20.1 MPa) and strain was 59%.

Later on, a newer version of the material testing machine was used in the laboratory which was Instron 3367 to perform tensile and compressive testing. This machine was connected to the computer and the data will be recorded. The results were recorded in load and displacement format and later calibrated the results into stress and strain curve. The first two tensile tests recorded the maximum stress of 1.65 ksi (11.37 MPa) and 1.53 ksi (10.6MPa), and the maximum strains were 99% and 100% respectively. For both of these tests, strain rate was identical. Another tensile test was performed at a slower strain rate but the computer failed to record any data. The elongation of this specimen is approximately 300%. Thus, after running many tests at different strain rates, it shows that the polyethylene will deform better due sustained loading than impact loading.

Next, compressive tests were performed at a different strain rate on Instron 3367. From the first and second compressive test results, the maximum stress was 1.7 ksi (11.72 Mpa) and 1.8 ksi (12.41 MPa) and maximum strain was 13% and 15 % respectively. In all these compressive tests, the test was stopped before the buckling had occurred. The results obtained are shown in Tables 2.1 and 2.2. Lastly, strain jump test was conducted and the results are presented in Table (2.2). The strain rate sensitivity is 0.344. Figures 2.5 through 2.9 depict the graphical comparison of the tests conducted.

Table (2.1): Tensile and Compressive Test Results

Instron	Strain rate	Testing Type	Test number	Max. Stress, ksi [MPa]	Max. Strain
1125	1×10^{-4}	Tension	1	1.315295 [9.1]	0.210261
1125	1×10^{-2}	Tension	2	2.914604 [20.1]	0.593327
3367	1×10^{-2}	Tension	1	1.652176 [11.4]	0.999998
3367	1×10^{-2}	Tension	2	1.525932 [10.5]	1.000001
3367	2×10^{-4}	Compression	1	1.718606 [11.8]	0.134847
3367	5×10^{-3}	Compression	2	1.877607 [12.9]	0.155643

Table (2.2): Strain Jump Test Results

Instron	Strain jump	Testing type	Test number	Max. stress, ksi (MPa)	Max. strain
1125	5×10^{-3}	Tension	1	0.496048 [3.4]	0.248421
1125	1×10^{-2}	Tension	1	0.809298 [5.6]	0.286682
1125	5×10^{-2}	Tension	1	1.314025 [9.0]	0.372942
1125	1×10^{-1}	Tension	1	1.538242 [10.6]	0.452349
1125	2×10^{-1}	Tension	1	1.827732 [12.6]	0.549277
1125	5×10^{-1}	Tension	1	2.271963 [15.6]	0.696641
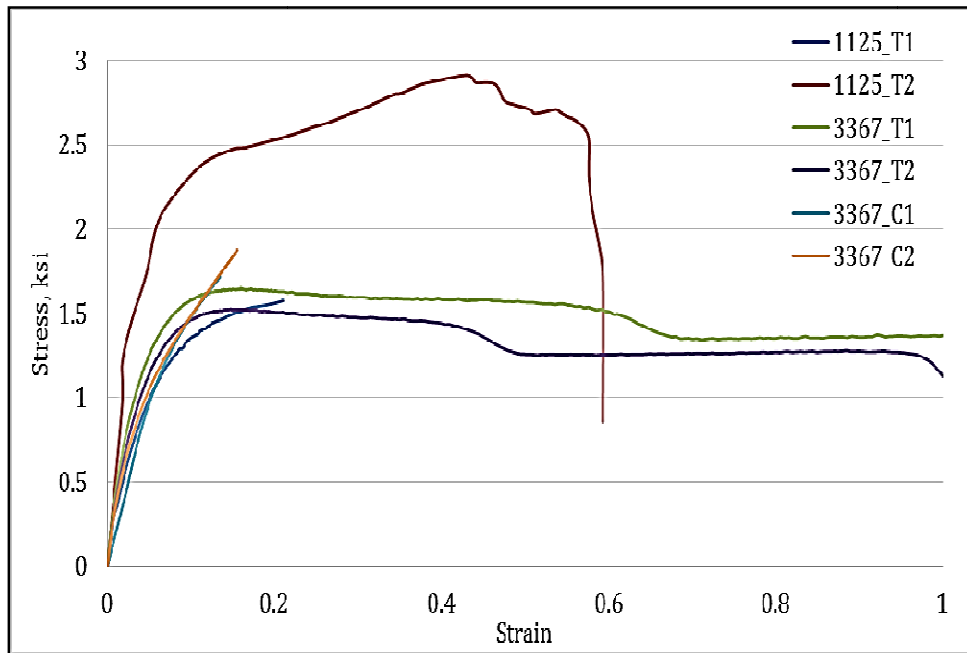
Figure (2.5): All Tensile and Compressive Testing of LDPE
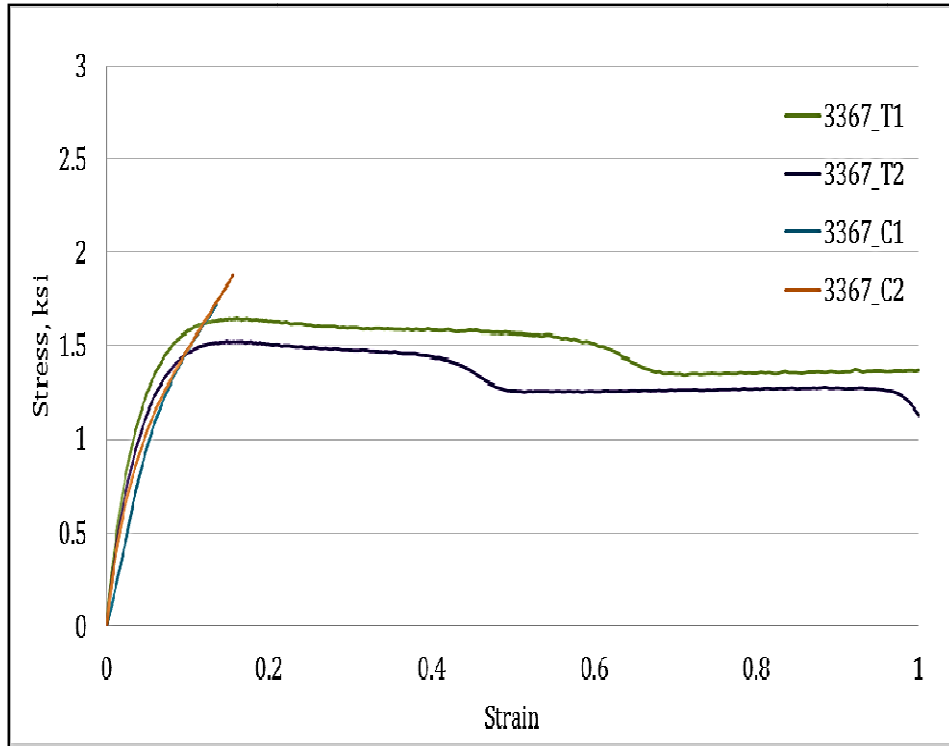
Figure (2.6): Instron 3367 Tensile/Compressive Testing of LDPE
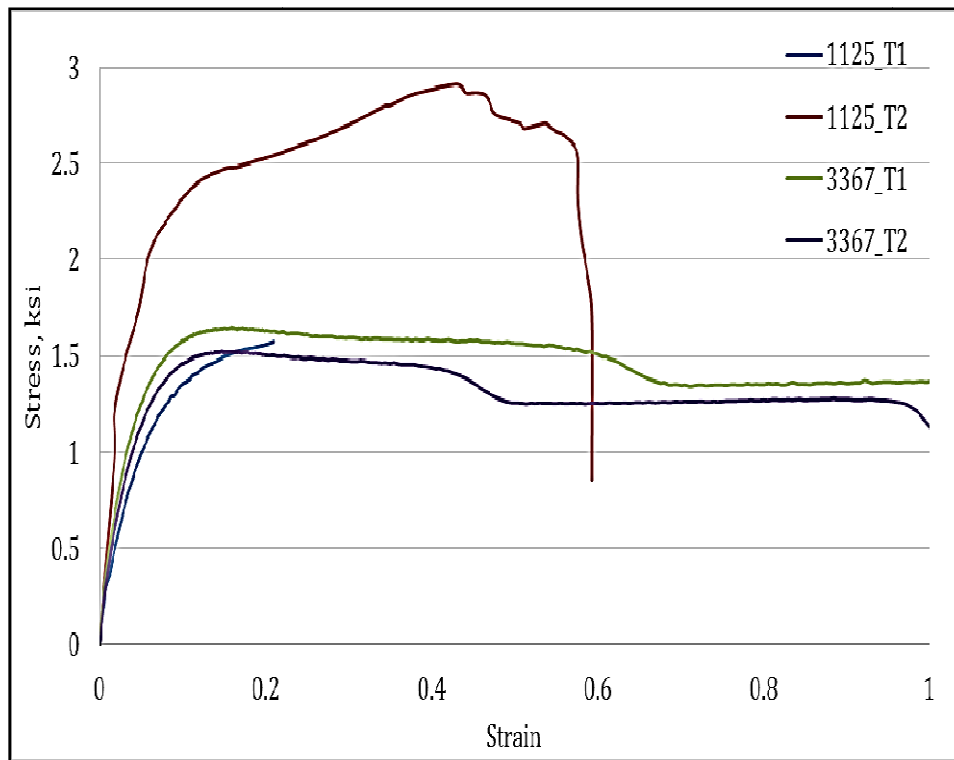
Figure (2.7): Tensile Testing on Instron 1125 vs. 3367
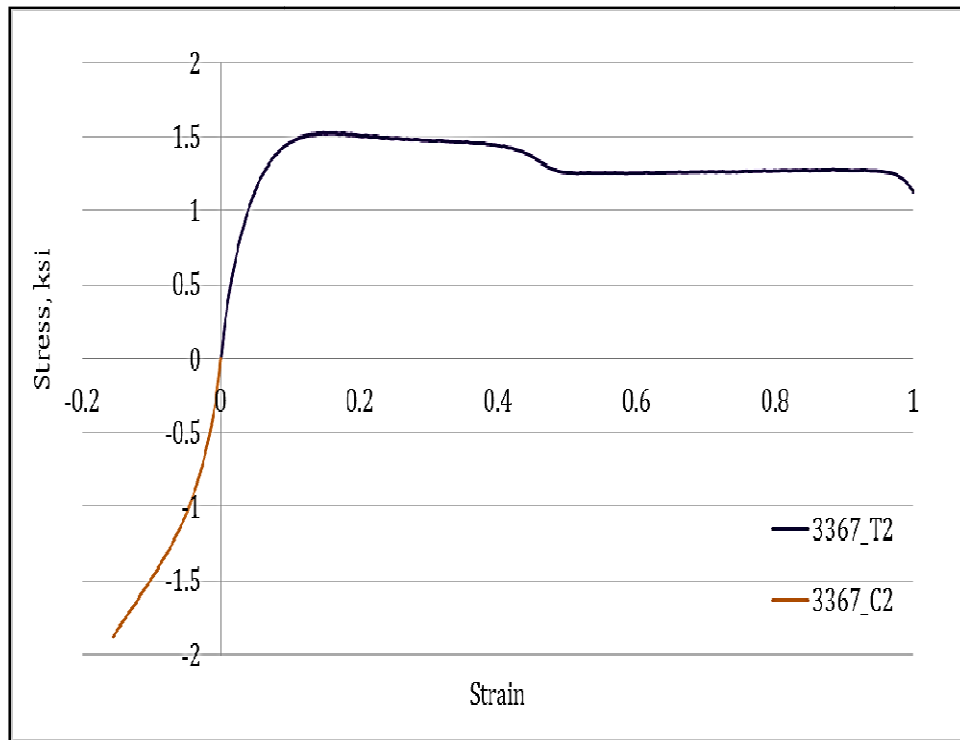
Figure (2.8): 3367_Tensile_2 vs. Compressive_2
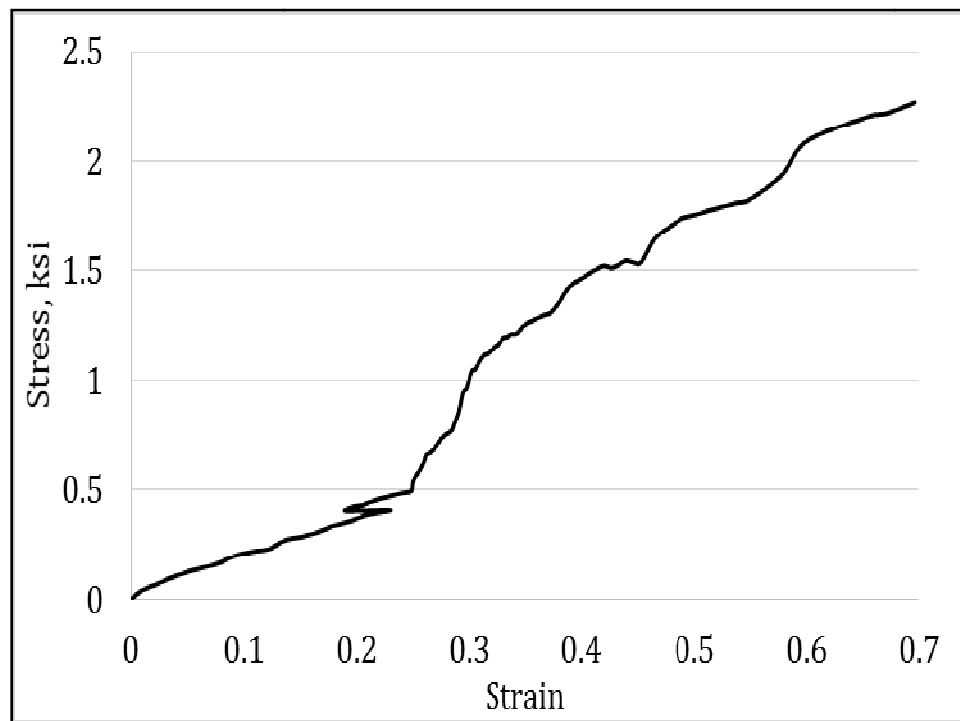
Figure (2.9): Strain Jump Test

13

2.3 DESCRIPTION OF EXPERIMENTAL PROGRAM
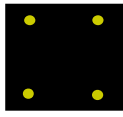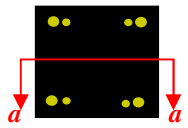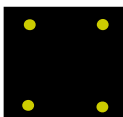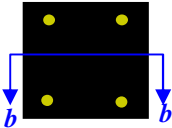
2.3.1 LDPE/FRP BEAMS TEST MATRIX
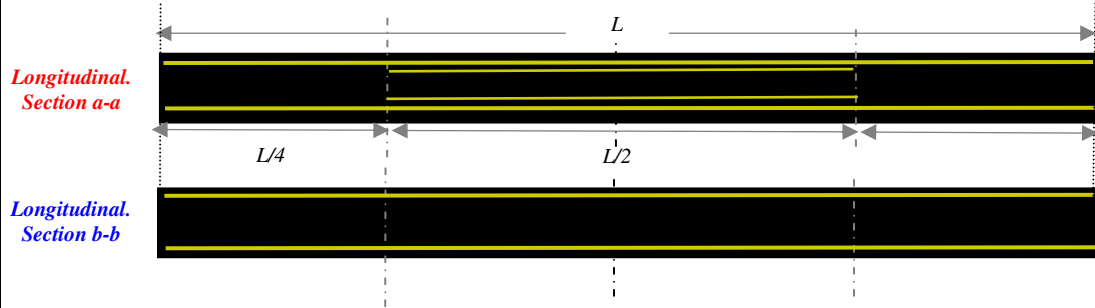
The hybrid LDPE/FRP composite beam specimens were manufactured by Plastic Pilings Incorporated (PPI) of California and were tested at the Structural Engineering Testing Hall (SETH) of the University of California, Irvine under the supervision of Professor Mosallam.

All large-scale tests were inspected prior to testing and measurements of each specimen were recorded. During all tests, displacement, strains and loads were continuously monitored and recorded during all tests using a computerized data acquisition system (DAS). The large-scale specimens were loaded under four point loading/unloading regime. This report summarizes the experimental results of two beam specimens that were tested under quasi-static loading/loading and loading-to-failure protocol.

Table (2.3) describes the test matrix for the full-scale beam specimens evaluated in this study. As shown in this table, two reinforcement details were investigated. Specimens PPI-B468 was reinforced with 4-#8 (1″/25.4mm diameter) E-glass/polyester FRP composite rebars extended along the whole length of the beam, while additional reinforcement of 4-#6 FRP rebars were installed at an equal distance of L/4 from each support (total length = L/2 as shown in Table (2.3). Specimens PPI-B408 was reinforced only with 4-#8 (1.0″/25.4mm diameter) E-glass/polyester FRP rebars extended along the whole length of the beam specimen with no additional reinforcement at the central region.

Table (2.3): Test Matrix [Source: Mosallam (2005)]

Specimen ID	Clear Span, *L*, inches [m]	Cross-section inches [mm]	Internal Reinforcement	
			Along Beam Length	At the ¼ Mid-span
PPI-B468*	150.75" [3.83 meters]	10" X 10" [254 mm X 254 mm]	4-#8	4-#8 + 4-#6
PPI-B408**	150.75" [3.83 meters]	10" X 10" [254 mm X 254 mm]	4-#8	4-#8

Longitudinal. Section a-a

Longitudinal. Section b-b

L   L/4   L/2

 * Cover = 1″ (25.4 mm)   **Cover = ¾″ (19 mm)

2.3.2 DATA AQUISITON SYSTEM (DAS)

A computerized data acquisition system (DAS) is used in measuring electrical or physical phenomenon such as voltage, current, temperature, pressure, or sound with a computer. A DASsystem consists of sensors, measurement hardware, and a computer with data acquisition software.   As compared to traditional measurement systems, PC-based DASsystems exploit the processing power, productivity, display, and connectivity capabilities of industry standard computers providing a more powerful, flexible, and cost-effective measurement solution. Parts of a data acquisition system are described below.

a) Electronic Sensors: The measurement of a physical phenomenon, such as the temperature of a room, the intensity of a light source, or the force applied to an object, begins with a sensor. A sensor, also called a transducer, converts a physical phenomenon into a measurable electrical signal. Depending on the type of sensor, its electrical output can be a voltage, current, resistance, or another electrical attribute that varies over time. In this case the electrical output was voltage.

b) DAS Boards and Devices: The DAS hardware acts as the interface between a computer and signals from the outside world. It primarily functions as a device that digitizes incoming analog signals so that a computer can interpret them. The three key components of a DASdevice used for measuring a signal are the signal conditioning circuitry, analog-to-digital converter (ADC), and computer bus. Many DASdevices include other functions for automating measurement systems and processes. For example, digital-to-analog converters (DACs) analog signals, digital I/O lines input and output digital signals, and counter/timers count and generate digital pulses. Figures (2.10) and (2.11) show the data acquisition system used and the connections of strain gauges and string potentiometers to the data acquisition system.
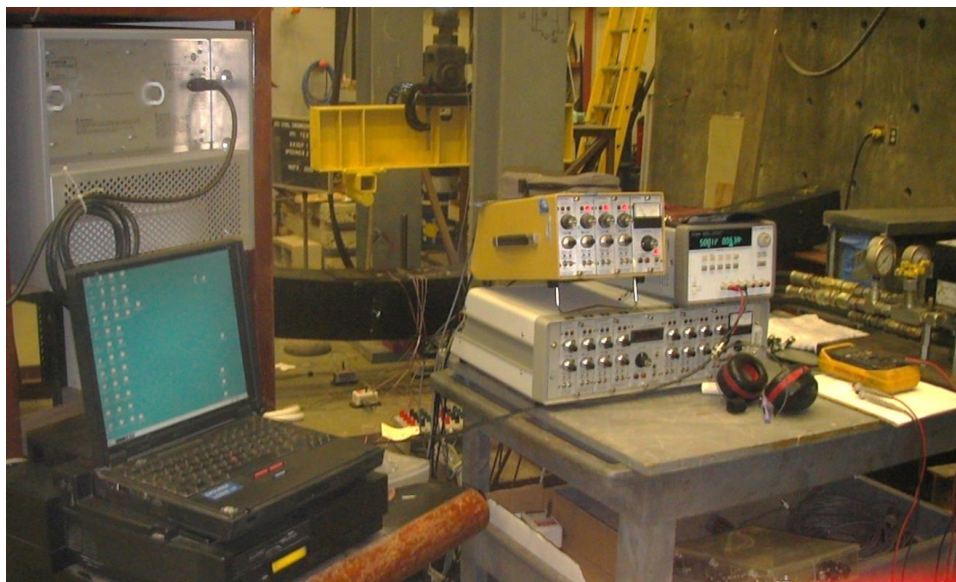
Figure (2.10): Data Acquisition System with National Instruments Channel

Figure (2.11): Load, deflection and strain data continuously and automatically recorded using a computerized data acquisition system

2.3.3 LOADING APPARATUS (THE HYDRAULIC ACTUATOR)

The hydraulicactuator used in loading all beam specimens was an MTS calibrated servo-hydraulic actuator model #244.31 with a capacity of 55.0 kips (244.65 kN). The actuator was mounted vertically onto a steel frame that was connected with post-tensioned rods into the laboratory's strong floor (Figure 2.12). The monotonic unidirectional load was applied, via a steel transfer beam connected to two steel cylinders applying the load to the specimen. The MTS actuator incorporated a 55-kip (244.65 kN) load cell and 40-inch (101.6 cm) displacement transducer. Both devices were calibrated and supported traceable certificates. The computer controlled hydraulic actuator is equipped with a load cell to measure the applied load and a displacement transducer to measure the movement of the actuator (Figure 2.13).
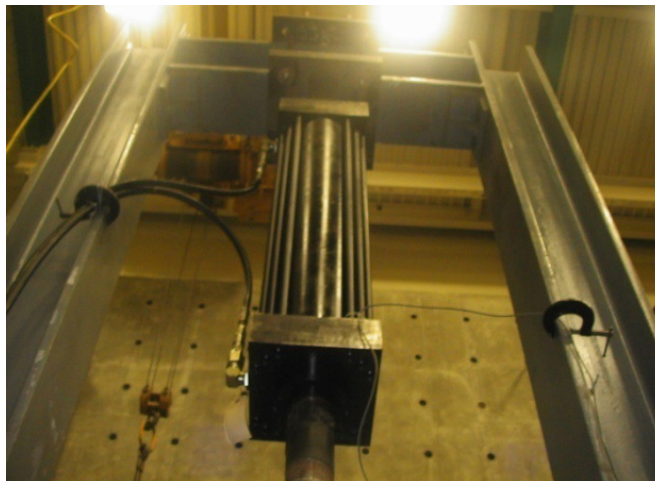
Figure (2.12): The HydraulicActuator Used in Applying the Monotonic Load

Figure (2.13): Typical 4-point beam test setup

2.3.4 ELECTRONIC STRING POTENTIOMETERS (STRING POTS)

String potentiometers (String pots) were attached to bottom surface of the hybrid beam to determine the deflection of specimen at locations determined by yield line theory. The locations of the string potentiometers attached are shown in (Figure 2.14).

Electronic String Potentiometers

Figure (2.14): Locations of String Potentiometers

2.3.5 ELECTRONIC STRAIN GAUGES

Electronic strain gauges were bonded to the top, bottom and also on the side surfaces of the composite beam (Figure 2.15). The strain gauges measure the strains at different locations in the specimen. These measurements are collected and stored in the DAS.All the strain gauges and the string pots wereconnected to differentDAS channels by conducting wires. Proper naming of the locations of the electrical components were done and noted prior to the start of the experiment. The same nomenclature was followed throughout the experiments and also in the analysis. Figure (2.16) shows the locations of differentstrain gages bonded to the mid-span section of the LDPE/FRP beam surface.
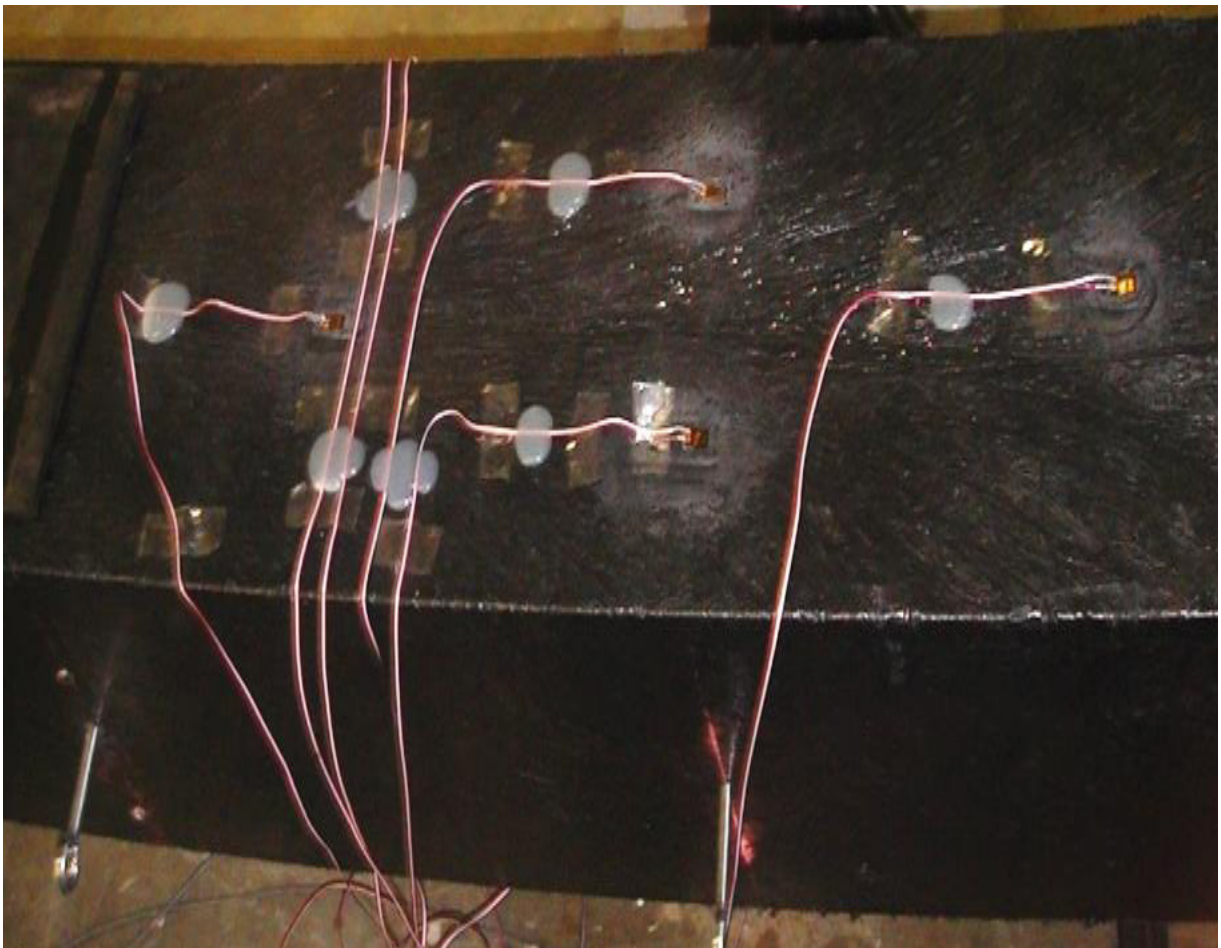
Figure (2.15): Locations of Strain Gauges
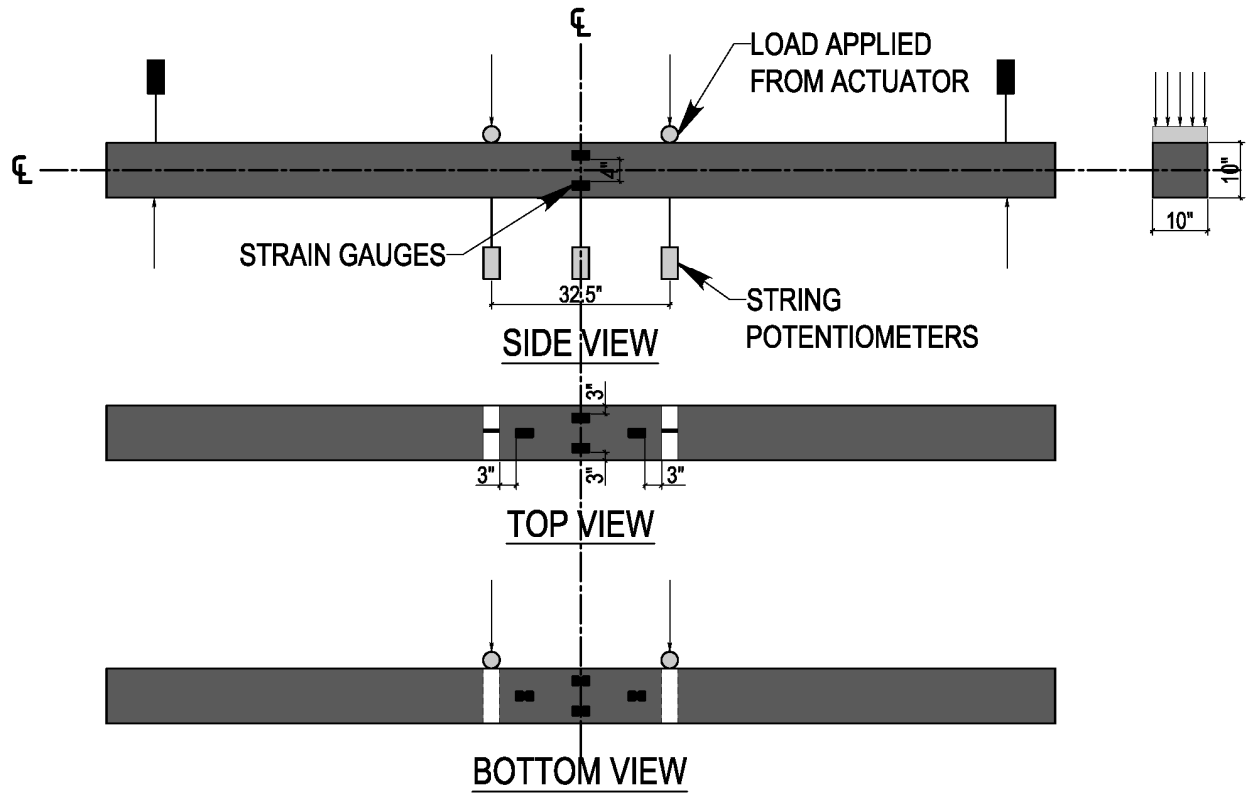
Figure (2.16): Locations of Strain Gauges and String Pots

CHAPTER 3

MECHANICAL BEHAVIOR OF HYBRID BEAM SPECIMEN

3.1 TEST MATRIX AND SPECIMEN DETAIL

3.1.1 LDPE PLASTIC MATRIX

Two tests were conducted to extract short-term mecahnical properties of LDPE plastic matrix. Figure (3.1) shows the coupon specimens used in charectriziaon tests. Table (3.1) shows the LDPE coupon test results. From the graph, Young's modulus/ modulus of elasticity can be calculated. It is the highest point attained before the line begins to curve. The intersection of the highest point of the straight line on the x-axis and y-axis is the modulus of elasticity (Figure 3.2).

$$Modulus\ of\ Elasticity, E(ksi[MPa])\ \ = \frac{Linear\ Stress\ (ksi[MPa])}{Linear\ Strain}$$

$$E = \frac{1.2}{0.06} = \mathbf{20}\ ksi\ (137.9\ MPa)$$
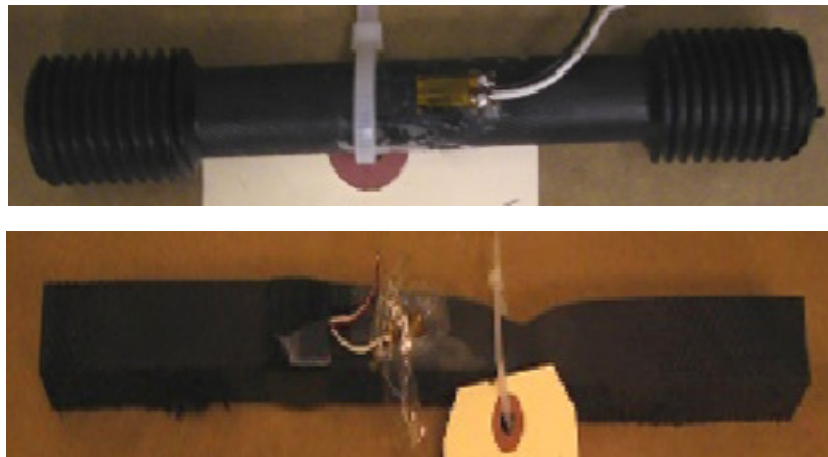
Figure (3.1): Coupon Specimens Used in Mechanical Characterization Tests
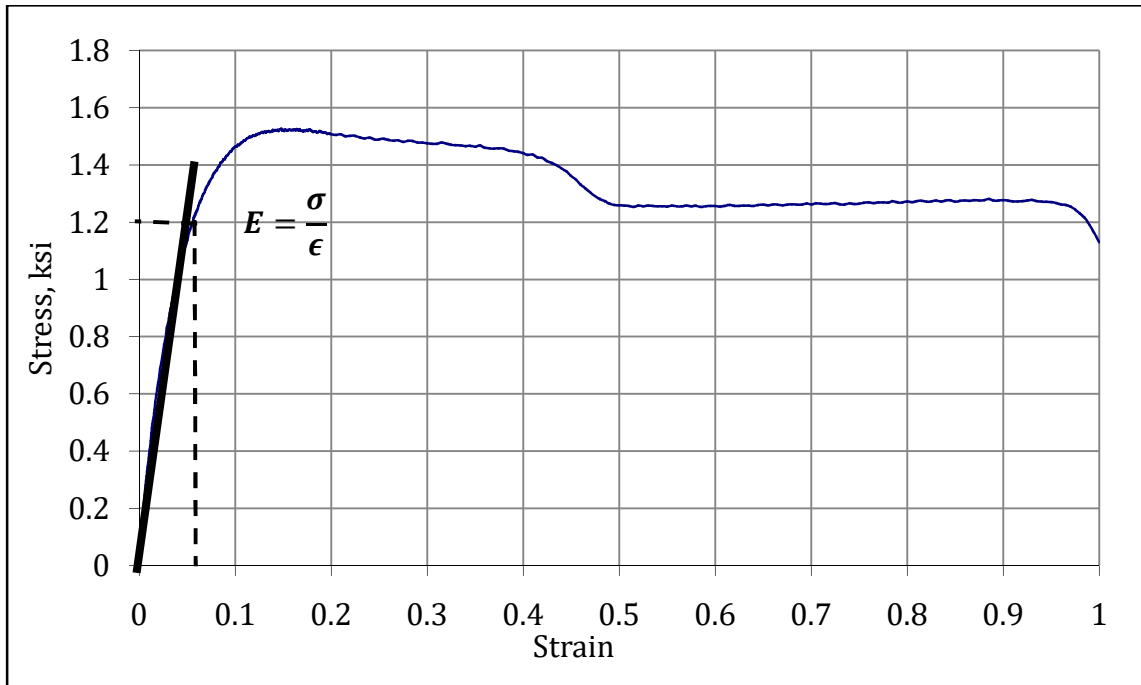
Figure (3.2): Modulus of Elasticity for LDPE from Coupon Tests

Table (3.1): LDPE Coupon Test Results

Average Modulus of Elasticity (E), ksi [MPa]	Average Tensile Strength, σ_u, ksi [MPa]	Average Rupture Strain, ϵ_u(%)
20ksi [137.89 MPa]	1.335ksi [9.20 MPa]	13.54

3.1.2 E-GLASS/POLYESTER FRP REBARS

The rebars used as internal reinforcement was made of pultruded E-glass/polyester composites, with an average fiber fraction of 60%. The mechanical properties of the rebars are shown in Table (3.2).

Table (3.2): E-Glass/ Polyester FRP Mechanical Properties

Bar Size	Bar Diameter, Φ inches [mm]	On-axis Tensile Strength, σ_{u11} ksi [MPa]	Modulus of Elasticity, E_{11} ksi [MPa]	Average Rupture Strain, ϵ_{u11}(%)
#8	1 [25.4]	87 [597]	6,073 [41.9]	1.59
#6	¾ [19]	95 [656]	6,680 [46.1]	1.58

3.2 BEAM TEST ASSEMBLY

3.2.1 GENERAL

The testing assembly used to apply the line loads to the test specimen's top surface is illustrated in Figure (3.4). As shown in the figure, the beam specimens were simply supported with a clear span of 150.75"(3.83 m). The test was conducted in a four-point loading regime in order to develop a constant moment region with zero shear between the applied line loads. This was essential for the analysis so that the beam theory formulation is applicable. The same test setup was used for all specimens.
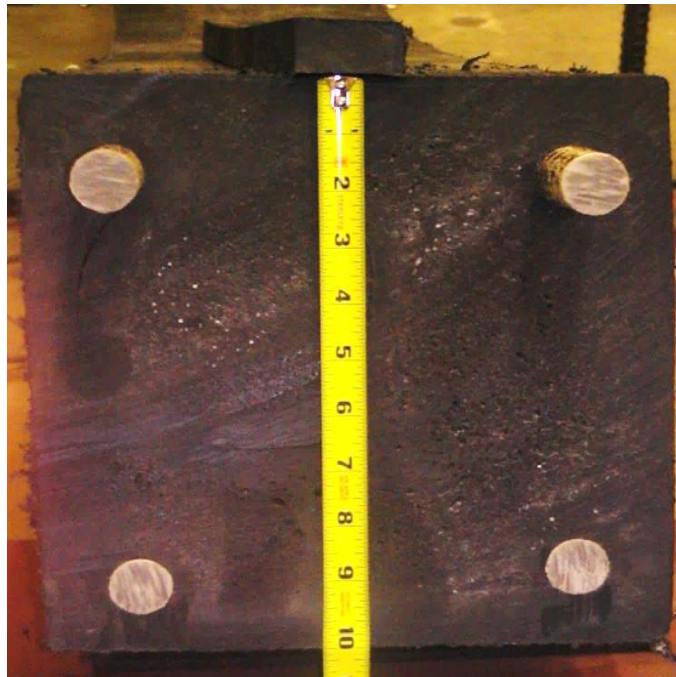
Figure (3.3): Cross-sectional view & slippage of GFRP Rebars at the ends of specimen

3.2.2 INSTRUMENTATION AND LOAD HISTORY

Each specimen was instrumented with electronic strain gages at different critical locations. Figure (3.4) shows the typical beam test setup that also shows the locations of strain gauges, as well as the deflection gauges. As shown in this figure, six string potentiometers were used to record the vertical deflection at the center as well as at the loading lines. As mentioned earlier, strain gauges were attached to the top, bottom and sides to measure the strain in the specimen during loading. Load, deflection and strain data were collected automatically and continuously using a computerized data acquisition system.

The load was applied using a 150.0 kips (672.0kN) hydraulic actuator with a 24.0″ (61.0 cm) stroke at a rate of 2.0 kips/minutes (8.90kN/minute). Loading/unloading regime was used up to about 50% of the ultimate load, after which a linear loading ramp was used up to the maximum load.

Figure (3.4): Typical four-point bending test setup

3.2.3 END SUPPORTS AND LINELOADS

As mentioned earlier, the beams were simply supported and were subjected to four-point loading. In order to avoid the development of stress concentration at the supports as well as the loading lines, elastomeric pads were placed under the beam ends covering the total width of the beam. This was also applied under the steel loading rods at the central region.

3.3 EXPERIMENTAL RESULTS

3.3.1 Beam Specimen PPI-B468

At first, beam dimensions were measured and recorded. Strain gages were attached to the top, bottom and sides of the beam specimens. The beam specimen was then carefully transported to the test area. Figure (3.5) shows the typical test setup of the beams.

During the loading/unloading cyclic phase, the behavior of this beam was linear with negligible permanent set. The behavior continued to exhibit near-linear behavior up to a load level of about 21.56 kips (95.63 kN), after which non-linear behavior initiated as shown in Figure (3.6). The full yield behavior was developed at a load level of about 23 kips (102.3 kN). Figures (3.7) and (3.8) show the linear behavior of this beam level at low stress levels of 5 kips and 10 kips, respectively. As shown in these figures, the highest value of linear stiffness was observed up to a load of 5.0kips (22.24kN) which is about 25% of the yield load and about 20% of the maximum load. At this level, the calculated flexural stiffness was 0.366×10^6 kip-in^2(2.5×10^6 MPa). The corresponding value at the load level of 10 kips (about 50% of the yield load and about 40% of the maximum load) was 0.3171×10^6 kip-in^2 (2.18×10^6 MPa). Detailed calculations for the flexural stiffness at different load levels are presented in Appendix at the end of this report.

At a load 22.5 kips (97.90 kN), the compression (top) FRP rebars began to slip from the plastic matrix. The slippage continued as the load increased and had reached to an average of 3¼" (82.6 mm) for the top reinforcement (Figure 3.2 and 3.10). However, a slight inward slippage was developed for the tensile (bottom) FRP rebars. (Figure 3.11)The ultimate load

of this specimen was 24.39 kips (108.50 kN), which is translated to a maximum moment capacity of 60.47 kip-ft (81.92 kN-m). The total energy absorbed by this beam is about 2.4 X 10^4lb-ft (3.25 X 10^4kN-m or 3.25 X 10^7 Joules). This appreciated energy capability is extremely beneficial for the intended application of such hybrid beams. After the test, careful inspection of the deformed specimen was performed. Based on visual observation, no local damage, indentation or matrix cracks were observed. However, the appreciable plastic deformation was irreversible upon removal of the load.

Applied Cyclic & Quasi-Static Loads
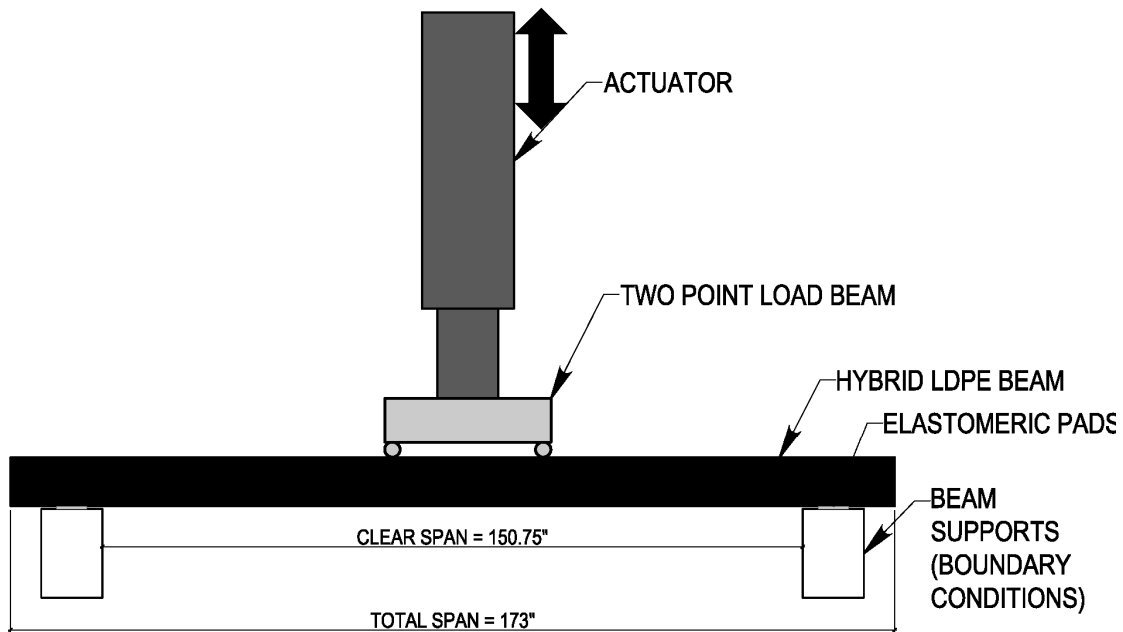
Figure (3.5): Typical Four-Point Bending Test Setup
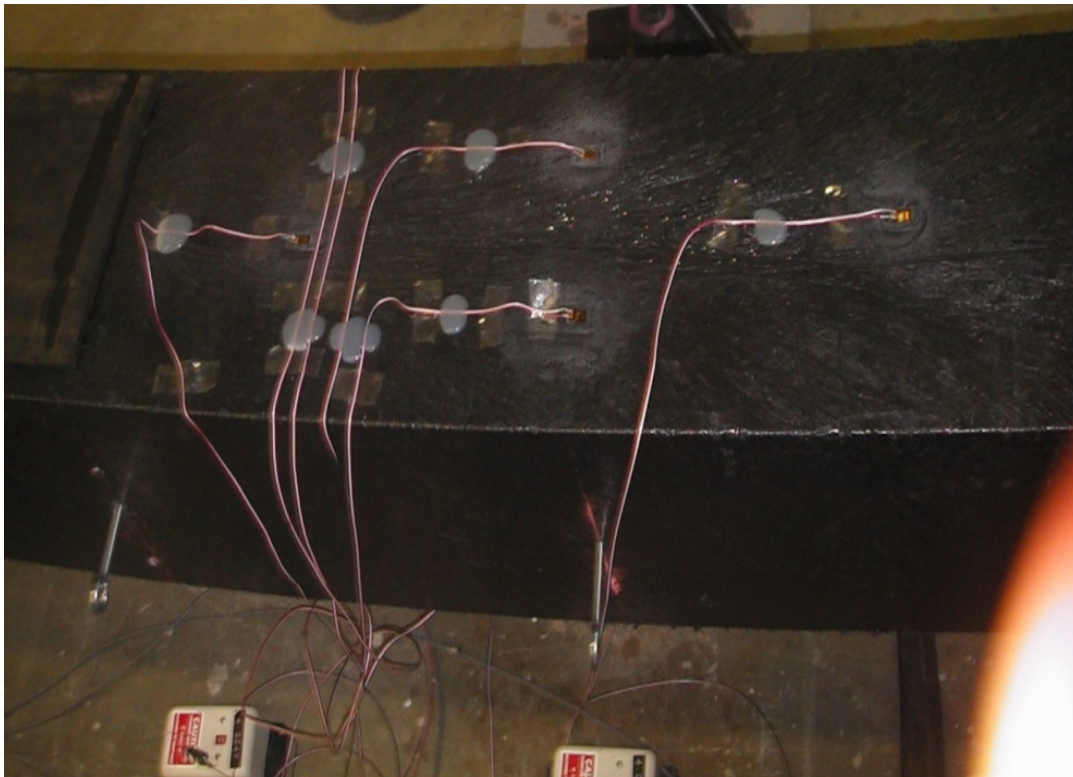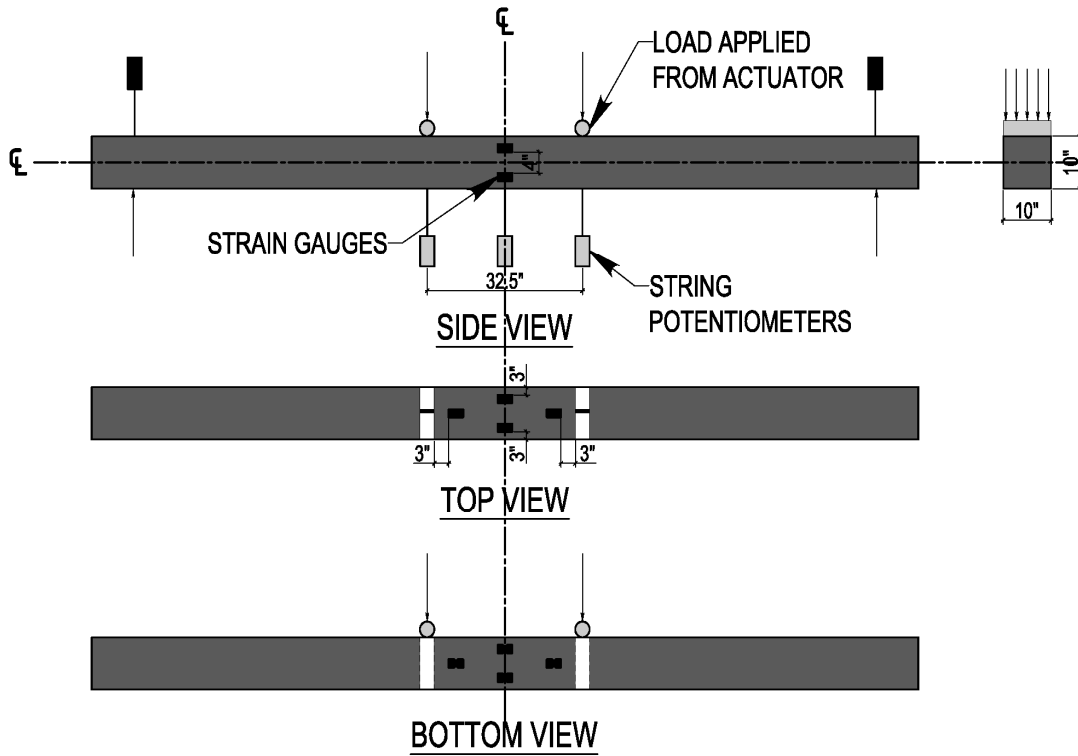
Figure (3.6): Locations of Strain and Deflection Gages
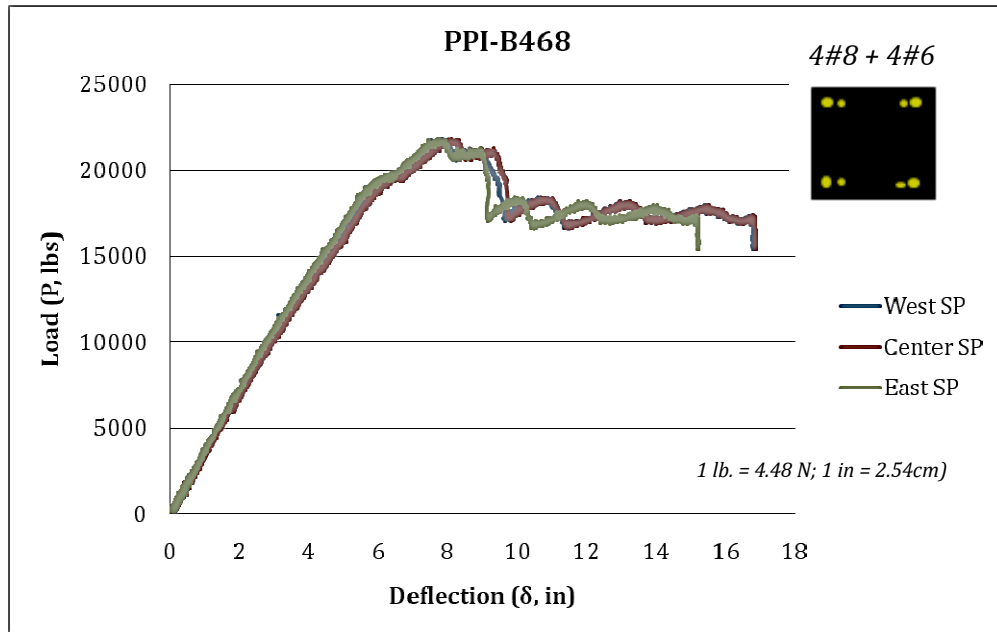
Figure (3.7): Load vs. Deflection Curve for Specimen **PPI-B468**
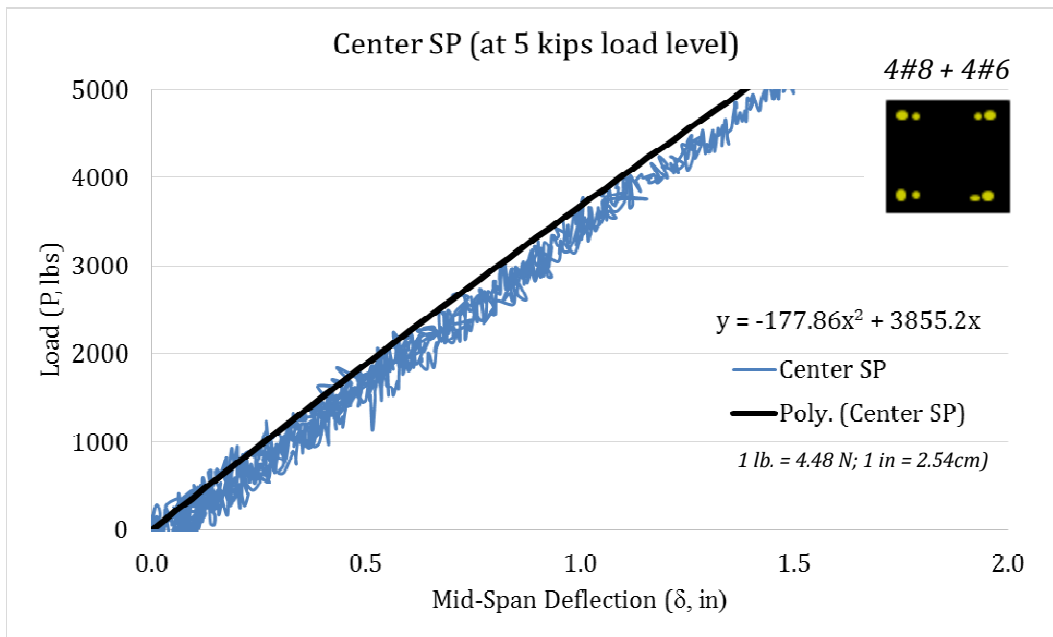
Figure (3.8): Load vs. Central Deflection at 5 kips (22.24 kN) load level for Specimen
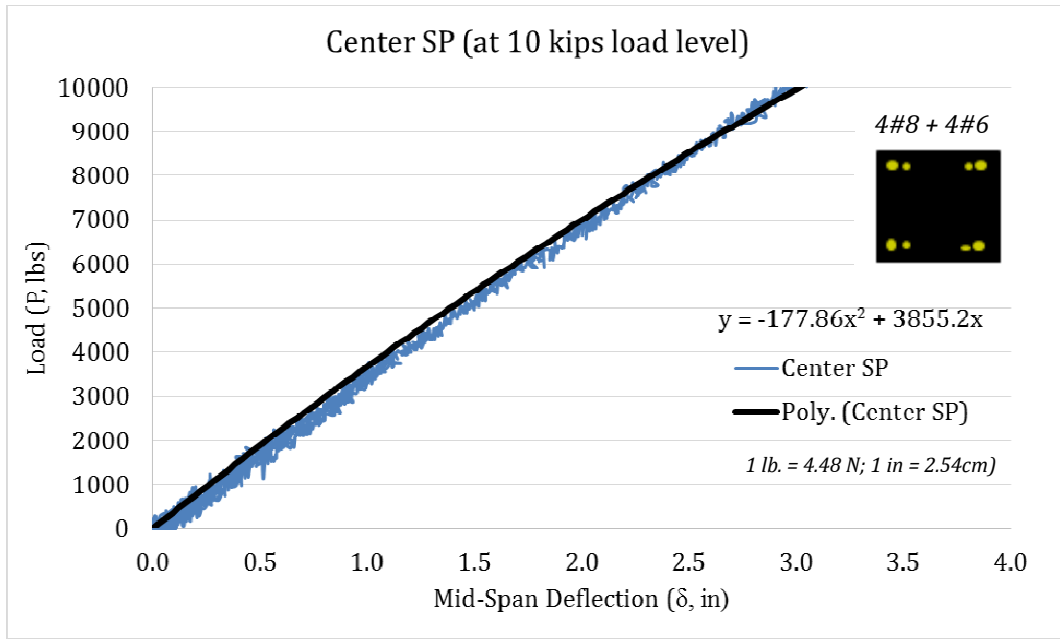
PPI-B468

Figure (3.9): Load vs. Deflection at 10 kips (44.48 kN) load level for Specimen **PPI-B468**
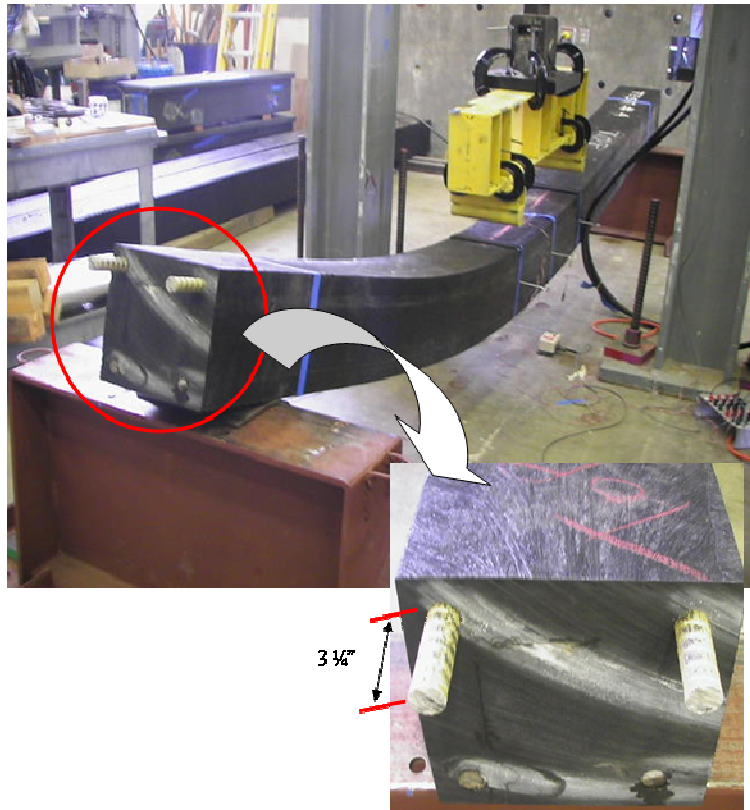
Figure (3.10): Slippage of FRP Rebars at the Ends of Specimen **PPI-B468**
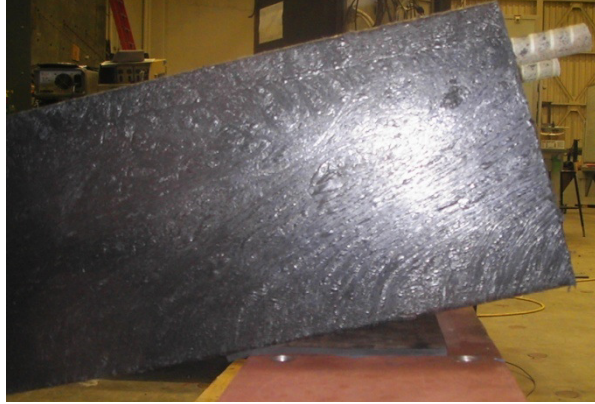
Figure (3.11): *a)* Displacement at the supports**,** *b)*Displacement at the mid span**,** *c)* Slippage of GFRP Rebars

3.3.2 Beam Specimen PPI-B408

Similar to the previous specimen, pre-test inspection, measurements confirmation and instrumentation were performed on this specimen prior loading. As mentioned earlier,

only 4#8 (4# 30mm) GFRP rebars were used to reinforce the bottom and the top sides of the beam.

During the loading/unloading cyclic phase, and similar to specimen PPI-B468, the behavior of this beam specimen was near-linear with negligible permanent sets up to a load level of 10 kips (44.48 kN). The behavior continued to exhibit linear behavior up to a load level of about 18.35 kips (81.63 kN), after which a slight non-linearity was observed. At a load of 20.85 kips (92.74 kN), an increasing non-linearity was initiated. As shown in Figure (3.12), the full plastic behavior was reached at a load level of 24.19 kips (107.6 kN) and this plastic behavior continued until the end of the test. Figures (3.13) and (3.14) show the linear behavior of this beam level at low stress levels of 5.0 kips (22.24kN) and 10.0 kips (44.48kN), respectively. As shown in these figures, the highest value of linear stiffness was observed up to a load of 5.0 kips (22.24kN) was about 25% of the yield load and about 20% of the maximum loads for specimen PPI-B408. At this load level, the calculated flexural stiffness was 0.2828 X 10^6kip-in^2 (1.9 X 10^6 MPa). The corresponding value at the load level of 10.0 kips (44.48kN) was 0.2803 X 10^6 kip-in^2(1.86 X 10^6MPa), which is about 50% of the yield load and about 40% of the maximum load as for specimen PPI-B468) Detailed calculations for the flexural stiffness at different load levels are presented in Appendix (I).

This test was stopped due to a different reason other than exceeding the maximum actuator stroke as in the case of specimen PPI-B408. The reason of halting the test was due to a sudden lateral movement accompanied by a large lateral deformation of the beam. Prior to the occurrence of lateral instability, a crackling sound was heard, indicating a crashing of one of the rebars inside the plastic matrix. Based on continuous and close monitoring of the behavior of the GFRP rebars at the beam ends, it was noticed that the slippage was initiated at one of the corner's rebars followed by inward slippage of the two bottom bars that was subjected to an increasing tensile stresses. The outward relative slippage of the top rebar was about 1 ¼" (31.75 mm) at the maximum load while the inward slippage was unequal for the bottom FRP rebars. The left corner rebars is suspected to be the one generated the loud crackling sound, indicating its failure (Figure 3.12). This assumption was supported by the large inward slippage of this bottom rebar to a distance

of about 1 ¼" (31.75 mm), while the other bottom rebar inward slippage was only ¾" (19 mm).   At this point, the test was stopped for safety reasons. Figure (3.13) shows the sequence of events as the instability occurred.

No slippage

1 ¼" outward slippage @Max Load

1 ¼" inward slippage @ Max Load

¾" inward slippage @ Max Load
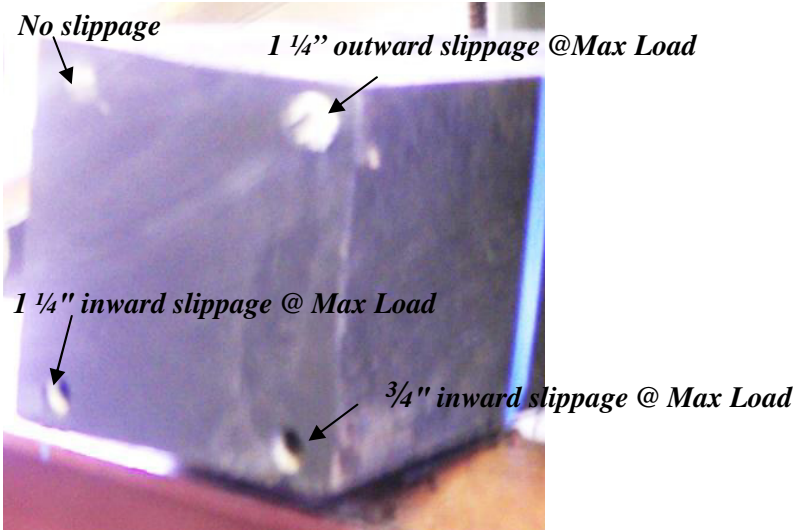
Figure (3.12): Uneven Slippage of the Corner FRP Rebars of Specimen **PPI-B408**
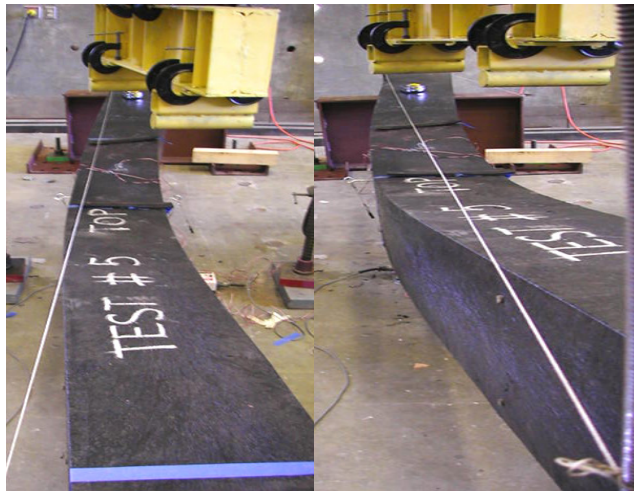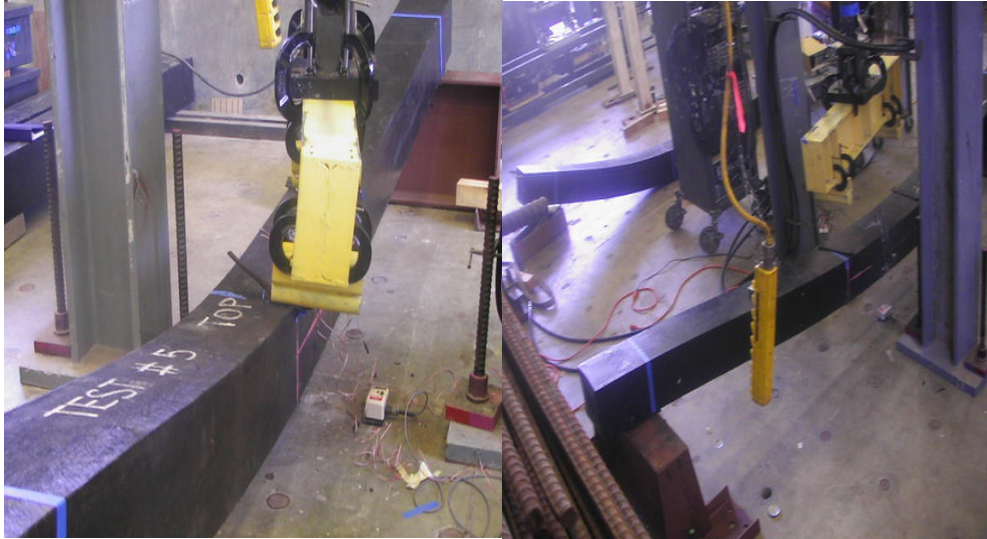
Figure (3.13): Lateral instability of beam specimen **PPI-B408**
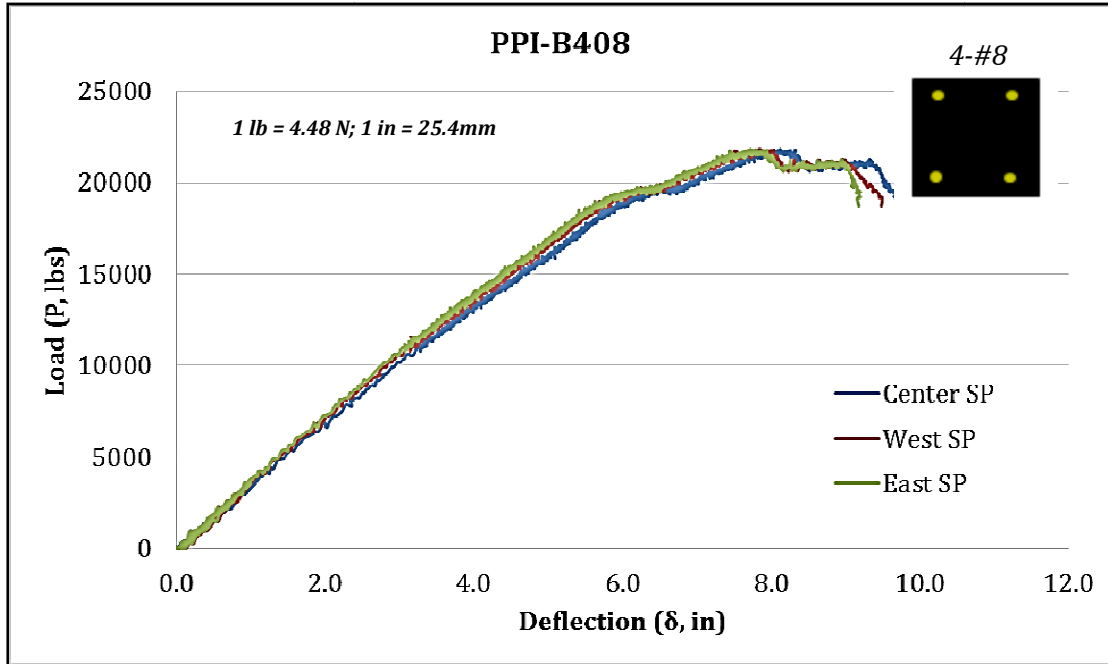
Figure (3.14): Load v/s Central Deflection for Specimen **PPI-B408**
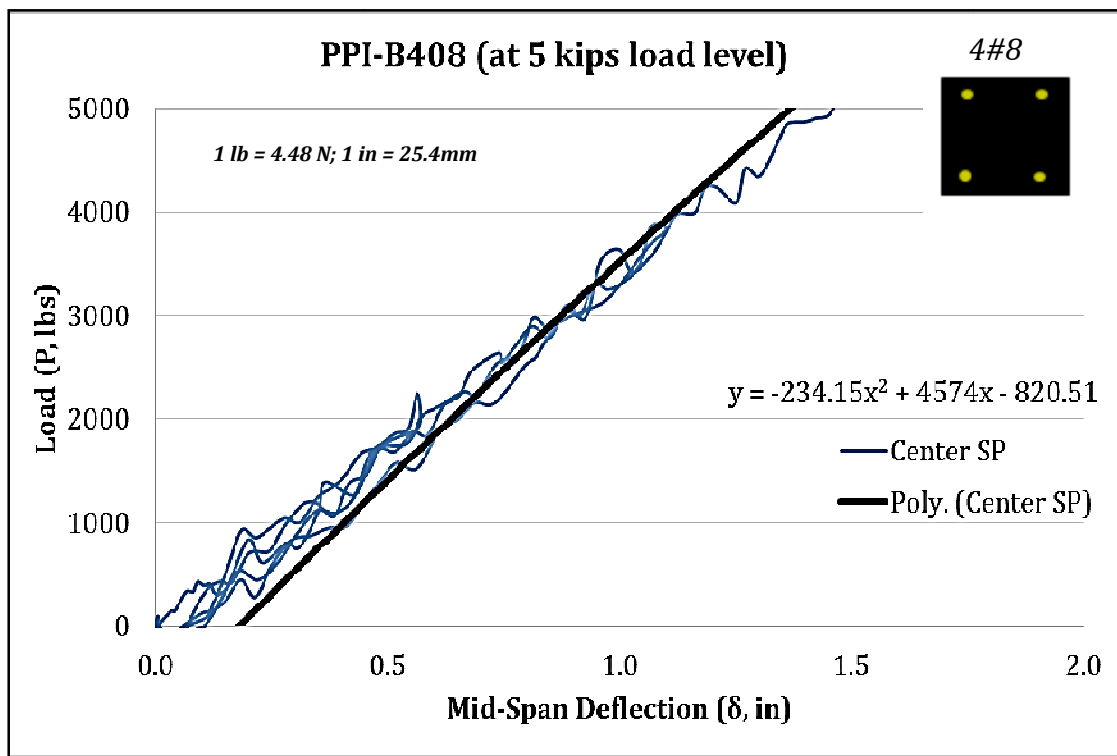
Figure (3.15): Load-Deflection Behavior of Specimen **PPI-B408** at **5-kip (22.24 kN)** Load Level
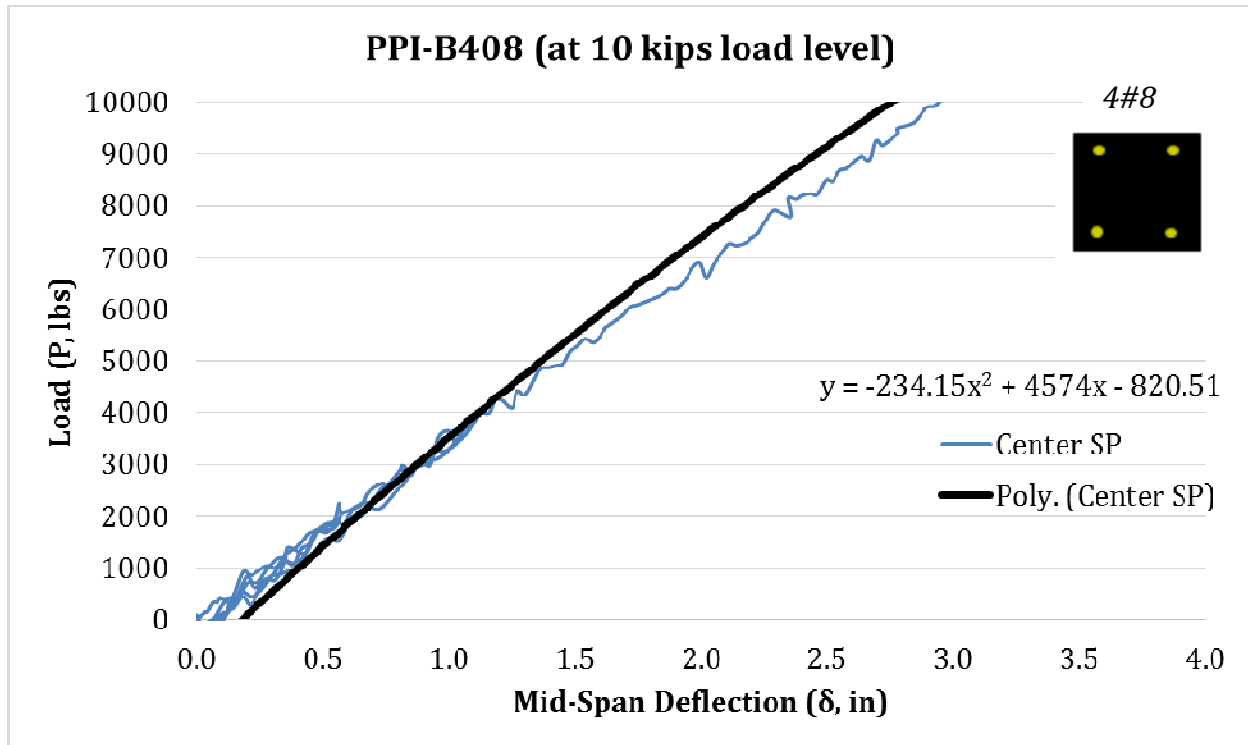
Figure (3.16): Load-deflection behavior of specimen **PPI-B408** at **10-kip (44.48 kN)** load level

Due to the hybrid nature of the beam specimens and the viscoelastic/elastoplastic behavior of the LDPE matrix, the flexural stiffness of the two beams, reported herein, was dependent on the stress level as well on the loading rate as expected. For example, beam specimen B408 has the maximum linear stiffness of 0.283 X 10^6kip-in^2 that occurredat a load level of 5 kips (22.24 kN). However, at a load level of 10.0 kips (44.5 kN), this value became 0.2802 X 10^6 kip-in^2 (1.9 X 10^6 MPa). At the beginning of the elastoplastic region (conservative value), the flexural stiffness was slightly reduced to 0.27 X 10^6 kip-in^2 (1.85 X 10^6 MPa) (about 1.88% of the target value of 0.276 X 10^6kip-in^2). So, up to a service load of 10 kips (about 50% of the yield load), the calculated stiffness exceeded the target value of 0.276X 10^9 lb-in^2 (1.9 X10^6). The change in the stiffness can also be attributed to the initial cyclic loading that was performed up to 10.0 kips (44.5 kN) which typically will result in a slight permanent set similar to the typical behavior of other construction materials including similar reinforced concrete members.

3.4 THEORETICAL ANALYSIS

The analytical modeling used in this study is based on a section analysis procedure developed by Mosallam (2005) that is similar to that used in the analysis of reinforced concrete beams. However, new parameters have been adopted for the hybrid beams based on available experimental data. The first part of the analysis is to define the material properties. The stress-strain curve for LDPE coupon specimens under compression and tension were shownearlier in Figure (2.8).Due to the fact that the LDPE matrix is free of cracks in tension region, an equivalent tension rectangular stress block is derived based on similar analysis to that of the compression equivalent rectangular stress block. Figure (3.17) shows the strain distribution as well as both the actual and proposedidealized stress distributions across the LDPE/FRP beam cross section.
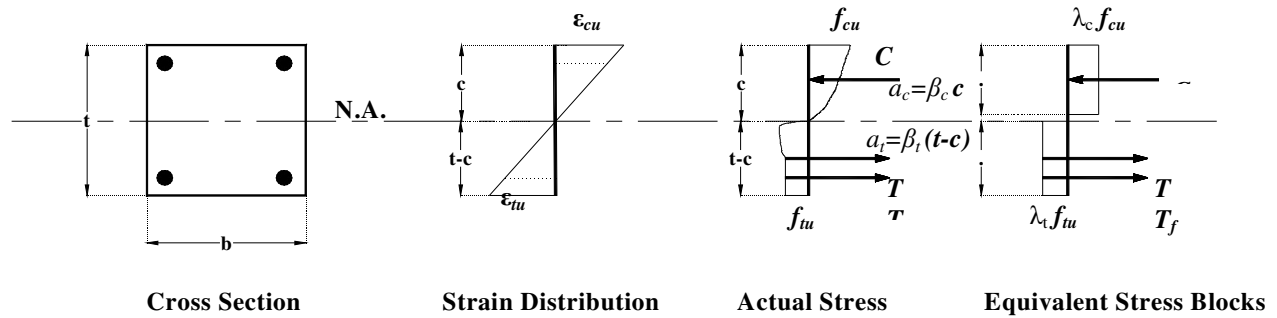
Figure 3.17: Stress-strain distribution for section analysis

The compression curve portrays a nonlinear parabolic relationship up to the maximum compressive strength, f_{cu}, at which the specimen reached the ultimate compressive strain, ϵ_{cu}(Figure 3.18). The plateau of compression stress-strain curve is assumed polynomial in the form:

$$f_c = 630.63\epsilon_c^3 + 202.11\,\epsilon_c^2 + 27.92\,\epsilon_c - 0.0833 \qquad \text{Eq. (1)}$$

The tension curve consists of four distinct regions: a parabolic relationship up to the maximum tensile strength, f_{tu}, and a linear descending branch up to a characteristic tensile strain, ϵ_{tp1}(Figure 3.19). The third region is a steeper linear plateau of the descending branch and it extends up to a characteristic tensile strain, ϵ_{tp2}. Finally, the forth region is a

flat constant profile with a constant stress level up to the ultimate tensile strain of ϵ_{tu} indicating the extreme ductility of the LDPE material.

The first region of the tensile stress-strain curve is assumed polynomial in the form:

$$f_t = A\,\epsilon_t{}^n + B\,\epsilon_t + C \qquad\qquad \text{Eq. (2)}$$

The four unknowns in Eq. (2) are determined from the following boundary conditions:

i. $ft = 0.0$ at $et = 0.0$

ii. $f_t = f_{tu}$ at $\epsilon_t = \epsilon_{to}$

iii. $df_t/d\epsilon_t = E_t$ at $\epsilon_t = 0.0$

iv. $df_t/d\epsilon_t = 0.0$ at $\epsilon_t = \epsilon_{to}$

$$\text{Eq. (3)}$$

The equations of tensile stress-strain relationship were determined to be:

For the first region:$0 < \epsilon_{t\,1} < \epsilon_{to}$

$$f_{t1} = E_t\epsilon_{t1}\,[1 - (1/n)\,(\epsilon_{t1}/\epsilon_{to})^{n-1}] \qquad\qquad \text{Eq.(4)}$$

$$n = (E_t\epsilon_{to})/(E_t\epsilon_{to} - f_{tu}) \qquad\qquad \text{Eq.(5)}$$

For the second region:$\epsilon_{to} < \epsilon_{t\,2} \le \epsilon_{tp1}$

$$f_{t2} = f_{tu} - E_{d1}\,(\epsilon_{t\,2} - \epsilon_{to}) \qquad\qquad \text{Eq.(6)}$$

$$E_{d1} = (0.93 f_{tu})\,/\,(\epsilon_{tp1} - \epsilon_{to}) \qquad\qquad \text{Eq.(7)}$$

For the third region:$\epsilon_{tp1} < \epsilon_{t\,3} \le \epsilon_{ttp2}$

$$f_{t3} = f_{tp1} - E_{d2}\,(\epsilon_{t3} - \epsilon_{tp1}) \qquad\qquad \text{Eq.(8)}$$

$$E_{d2} = (0.825 f_{tu})\,/\,(\epsilon_{tp2} - \epsilon_{tp1}) \qquad\qquad \text{Eq.(9)}$$

For the fourth region: $\epsilon_{tp2} \le \epsilon_{t\,4} < \epsilon_{tu}$

$$f_{t4} = 0.825 f_{tu} \qquad\qquad \text{Eq.(10)}$$

The parameters of the previous stress-strain curve are given as [2, 5]:

f_{tu} = 1526 psi (10.71 MPa); ϵ_{to} = 0.153 ; ϵ_{tp1} = 0.42 ; ϵ_{tp2} = 0.495 ; ϵ_{tu} = 0.975;

$E_{t=}$ 63.0 X 10³ psi (442.36 MPa)

f_{cu}= 1,878.0 psi (13.19 MPa);$\mathcal{E}_{cu}$= 0.1556

Based on experimental evidences, it is appropriate to assume the FRP composite rebars tobelinear elastic up to failure as shown in Figure (1.9). The properties of the FRP rebars are presented in Table (3.2).

The section analysis procedure proposed by Mosallam (2005) is based on the following assumptions:

- Tension zone matrix of LDPE is crack free,
- Tensile resistance of the FRP rebars can be neglected in the transverse direction,
- FRP rebar's compression resistance is neglected,
- Based on the experimental observations, the bond between the tension side FRP rebars and the LDPE matrix is maintained up to the final stage of loading (ultimate load), at which bond failure takes place simultaneously with the FRP rupture in tension, and
- Plane section before bending remains plane after bending, and hence a linear strain distribution can be assumed along the section, providing that some approximation to the nonlinearity of strain is accepted.

In order to proceed with section analysis, it is necessary to develop the parameters of the equivalent rectangular stress block shown in both compression and tensile zones of the cross section of the hybrid beams as indicated Figure (3.17). By integrating the stress-strain curve for LDPE coupon specimens in compression using Simpson's Rule, these parameters can be determined to be: β_c= 0.82 and λ_c= 0.79

Similarly, by Simpson's Rule integration of the stress-strain curve for LDPE coupon specimens in tension, the tension equivalent rectangular stress block parameters can be determined to be:β_t= 1.00 and λ_t= 0.857
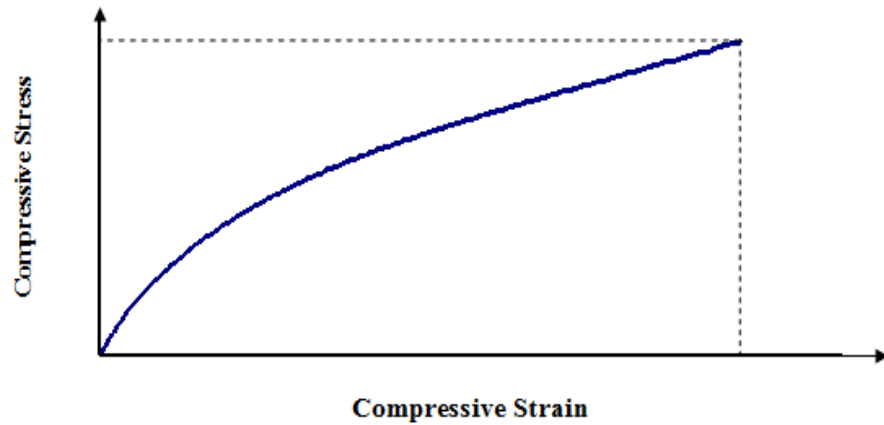
Figure (3.18): Stress-strain model for LDPE in *Compression*
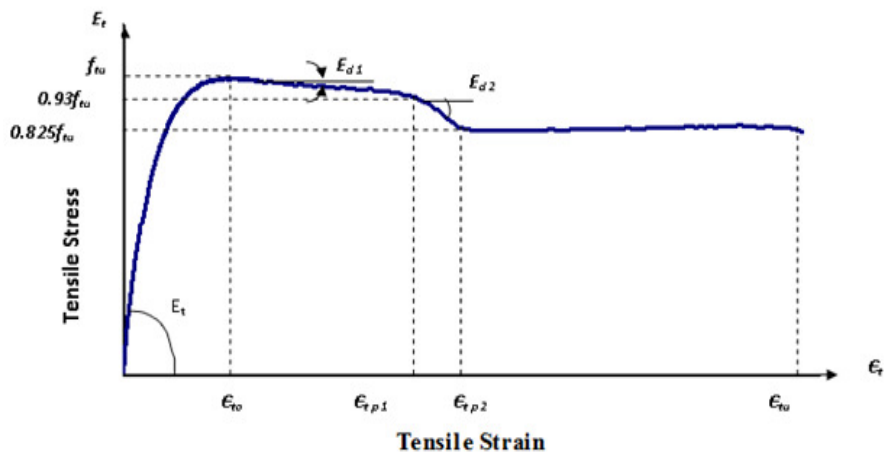
Figure (3.19): Stress-strain model for LDPE in *Tension*

The steps for calculating the ultimate moment and the maximum load for the two LDPE hybrid beams are as follow:

1- Beam PPI-B468

Calculation of neutral axis depth:

$t = b = 10$ *inch (25.40 cm)*

$a_c = \beta_c c = 0.82\ c$

$a_t = \beta_t(t-c) = t-c$

39

Materials and section properties:

LDPE Compression Force $C = a_c X \lambda_c f_{cu} X b$ = 0.82 c x 0.79 x 1.878 x 10 = 12.16568 c

LDPE Tension Force: $T = a_t X \lambda_t f_{tu} X b$ = 1.00 c x 0.857 x 1.526 x 10 = 13.07782 c

FRP Rebars Tension Force = $A_f f_f = A_f E_f \varepsilon_f$ = 2 x 0.785 x 6073 x ε_f + 2 x 0.441 x 6680 x ε_f = 17563.97ε_f

From strain compatibility:

$\varepsilon_f = \varepsilon_{cu} [(d-c)/c]$

T_f = 2732.95 x (9-c) / c

From static equilibrium:

$C = T + T_f$

Thus,

12.166 c = 13.078 c + 2732.95 x (9-c) / c

From which;

c = 9.027 in (22.93 cm), a_c = 7.40 in (18.80 cm) , a_t = 0.973 in (2.47 cm)

Calculation of ultimate moment:

Mu = C x (d-a_c/2) – T x [(t-c)/2-1]

M_u *(theoretical) = 642.65kip-inch = 53.55 kip-ft (73.94 kN-m)*

M_u *(experimental) = 60.47 kip-ft (83.44 kN-m)*

Mu (theoretical)/ Mu (experimental) = 0.89

2- Beam PPI-B408

Calculation of neutral axis depth:

t = b = 10 inch (254.0 mm)

$a_c = \beta_c c$ = 0.82 c

$a_t = \beta_t(t-c)$ = t-c

Material and section properties:

LDPE Compression Force C = a_c x $\lambda_c f_{cu}$ x b= 0.82 c x 0.79 x 1.878 x 10 = 12.16568 c

LDPE Tension Force T= a_t x $\lambda_t f_{tu}$ x b= 1.00 c x 0.857 x 1.526 x 10 = 13.07782 c

FRP Rebars Tension Force = $A_f f_f = A_f E_f \varepsilon_f = 2$ x 0.785 x 6073 x $\varepsilon_f = 9534.61 \varepsilon_f$

From strain compatibility:

$\varepsilon_f = \varepsilon_{cu} [(d-c)/c]$

$T_f = 1483.58$ x (9-c) / c

From static equilibrium:

$C = T + T_f$

thus,

12.166 c = 13.078 c + 1483.58 x (9-c) / c

fromwhich;

c = 9.05 in (22.99 cm), a_c = 7.21in (18.31 cm), a_t= 0.95 in (2.413 cm)

Calculation of ultimate moment:

$M_u = C$ x $(d-a_c/2) - T$ x $[(t-c)/2-1]$

M_u (theoretical) = 656.14 kip-inch = 54.67kip-ft (75.44 kN-m)

M_u (experimental) = 60.42 kip-ft (83.38 kN-m)

Mu (theoretical)/ Mu (experimental) = 0.90

Table (3.3): Summary of Theoretical Results

Specimen	Experimental Ultimate Moment M_u(exp) (kip-ft) /(kN-m)	Theoretical Ultimate Moment M_u (theo) (kip-ft) (kN-m)	Mu(theo) / Mu(exp)
PPI-B468	60.47 (83.44)	53.55 (73.94)	0.89
PPI-B408	60.42 (83.38)	54.67 (75.44)	0.90

CALCUALTIONS OF THE FLEXUARL STIFFNESS BASED ON FULL-SCALE TEST RESULTS

Appendix presents the actual stiffness values of the two beam specimens. The results of this analysis indicated that both beams have met the target flexural stiffness value of 0.27 X 10^9 lb-in^2 (0.789 X 10^6 N.m^2) that was set by Caltrans.

3.5 FINITE ELEMENT (FE) MODELING AND ANALYSIS (MARC-MENTAT)

3.5.1 INTRODUCTION ABOUT THE SOFTWARE

This chapter covers the finite element analysis of LDPE Hybrid beam using FE software MARC-MENTAT®. MARC-MENTAT®2015.0.1 is a software suite for finite element analysis and computer-aided engineering, originally released in 1971 by MARC® Analysis Research Corporation.MSC MARC-MENTAT® is nonlinear finite elements analysis software used to simulate behavior of complex materials and interaction under large deformations and strains.

It is a software application used for both the modeling and analysis of mechanical components and assemblies (pre-processing& post-processing) and visualizing the finite element analysis result. Engineering structures and systems often use nonlinear materials and experience complex interactions between various parts. For example, the stress-strain curve of an elastomer is highly nonlinear. During installation, elastomeric components could fold onto themselves and could undergo buckling. Their properties change with temperature and time. These nonlinearities are often grouped into three major categories, namely geometric, material and boundary condition nonlinearities. MARC® software is used to perform Finite Element Analysis of structures accounting for all these nonlinearities, in one, two and three dimensions. An example of a window screen at the start up is shown in Figure (3.20).

3.5.2 CREATING THE MODEL IN MARC-MENTAT® FE CODE

In this section, the numerical finite element model used in analyzing the Hybrid LDPE/FRP composite beam is discussed. The hybrid beams were made of LDPE and FRP Rebars were embedded in the beam (PPI-B408 and PPI-B468). The material properties of LDPE and FRP are discussed below. The boundary conditions are applied at the clear span (150.75"/3.82m) and at the bottom surface of the model as well as constraints within the model that determine the behavior of materials in contact with each other. The loading method applied to the model and its subsequent behavior is determined. The static loading conditions were applied to the models and analyzed. The results obtained from the

numerical analysis of test specimens are presented and comparisons between the numerical and experiment results are discussed. A step-by-step procedure and screenshots of the models have been included for better understanding of the analysis process.

It should be noted that the numerical analysis conducted in this study is limited to the service load-deflection range of the hybrid beams. As it was discussed in the experimental program, the ultimate failure was due to slippage between the FRP rebars and the matrix. Detailed analysis of the slippage failure mode is not included in the scope of this numerical study.
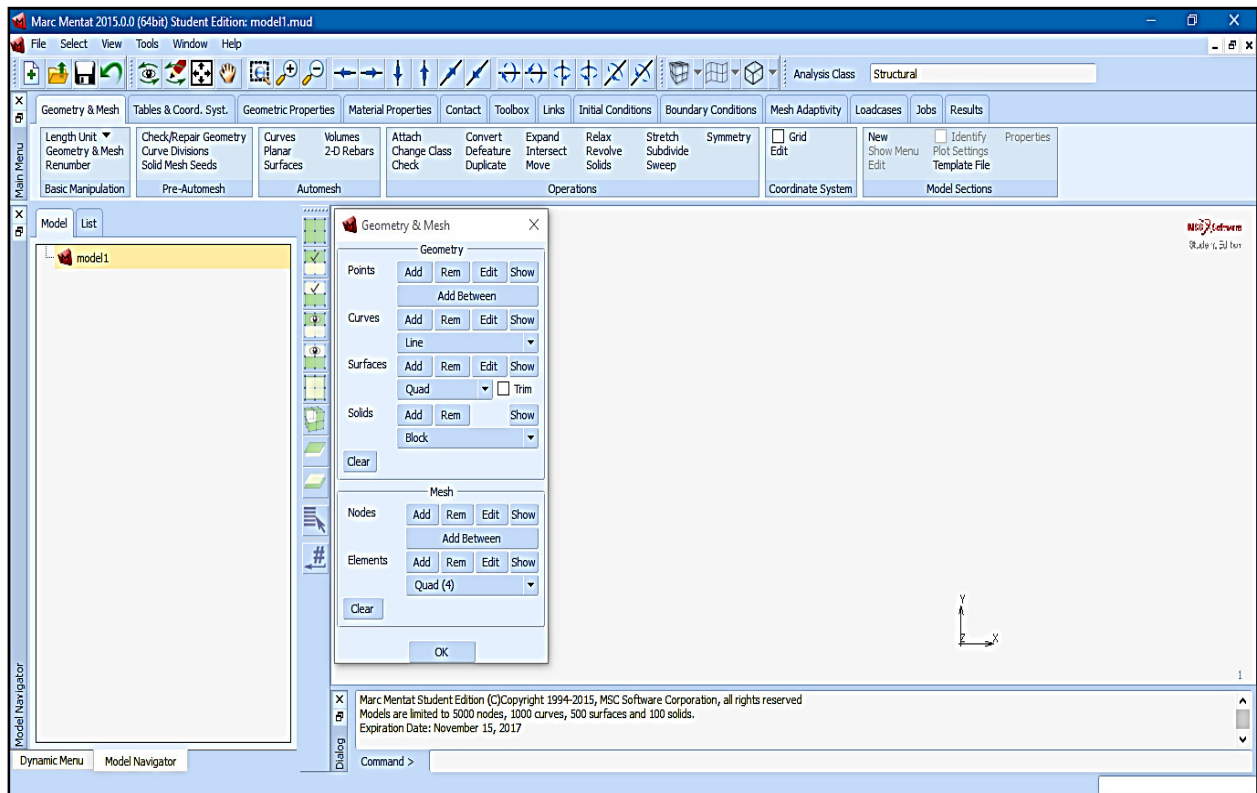
Figure (3.20):MARC-MENTAT® window screen

Low-Density Polyethylene Matrix (LDPE): As described earlier, the mechanical properties of the LDPE matrix were obtained from different coupon specimens teststhat were used in the numerical modeling (refer to Table 3.4).

Table (3.4): LDPE Coupon Specimen Mechanical Properties

Modulus of Elasticity (E) ksi [MPa]	Tensile Strength(σ_u) ksi [kPa]	Average Rupture Strain, ϵ_u (%)
63 ksi [434.369]	1.335 [9,204.5]	13.54

2) Fiber Reinforced Polymer Rebars: The mechanical properties of the E-glass/polyester FRP   composite rebars are presented in Table (3.5).

Table (3.5): E-Glass/ Polyester FRP Mechanical Properties

Bar Size	Bar Diameter, Φ inches [mm]	On-axis Tensile Strength, σ_{u11} ksi [MPa]	Modulus of Elasticity, E_{11} ksi [MPa]	Average Rupture Strain, ϵ_{u11} (%)
#8	1 [25.4]	87 [597]	6073 [41.9]	1.59
#6	¾ [19]	95 [656]	6680 [46.1]	1.58

3.5.3 STEP-BY-STEP PROCEDURE FOR CREATING THE FINITE ELEMENT MODEL

The dimensions and the mechanical properties are defined from the coupon tests and the experimental results. The LDPE beam is defined in the model by giving the coordinates for the exact dimensions and the boundary conditions with the location of the load application as per experimental data and is shown in Figure (3.21).The LDPE beam section selected is of 3D solid section beam. In MARC-MENTAT®, material properties are defined as shown in the Figure (3.22).In this model, the LDPE beam mesh was defined as hex element, while FRP rebars were defined as a wire element by giving exact dimensions and mechanical properties Figure (3.23). In this model, the FRP rebars are embedded into the LDPE beam as shown in Figure (3.24). The nodes of the FRP are connected to the nodes of LDPE quadrilateral elements.
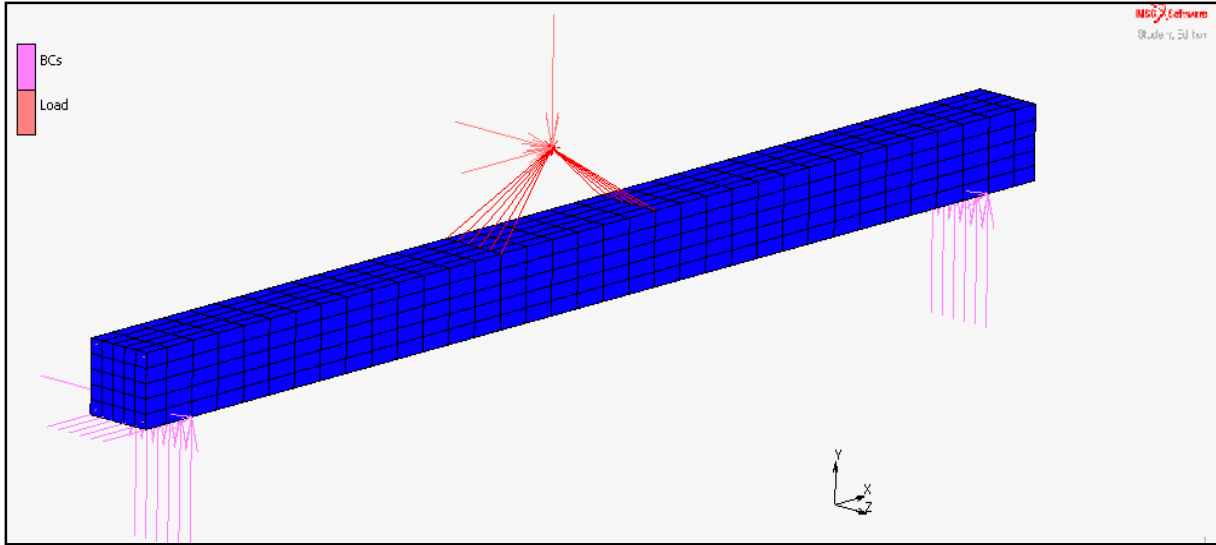
Figure (3.21): LDPE 3D solid section beam with boundary conditions
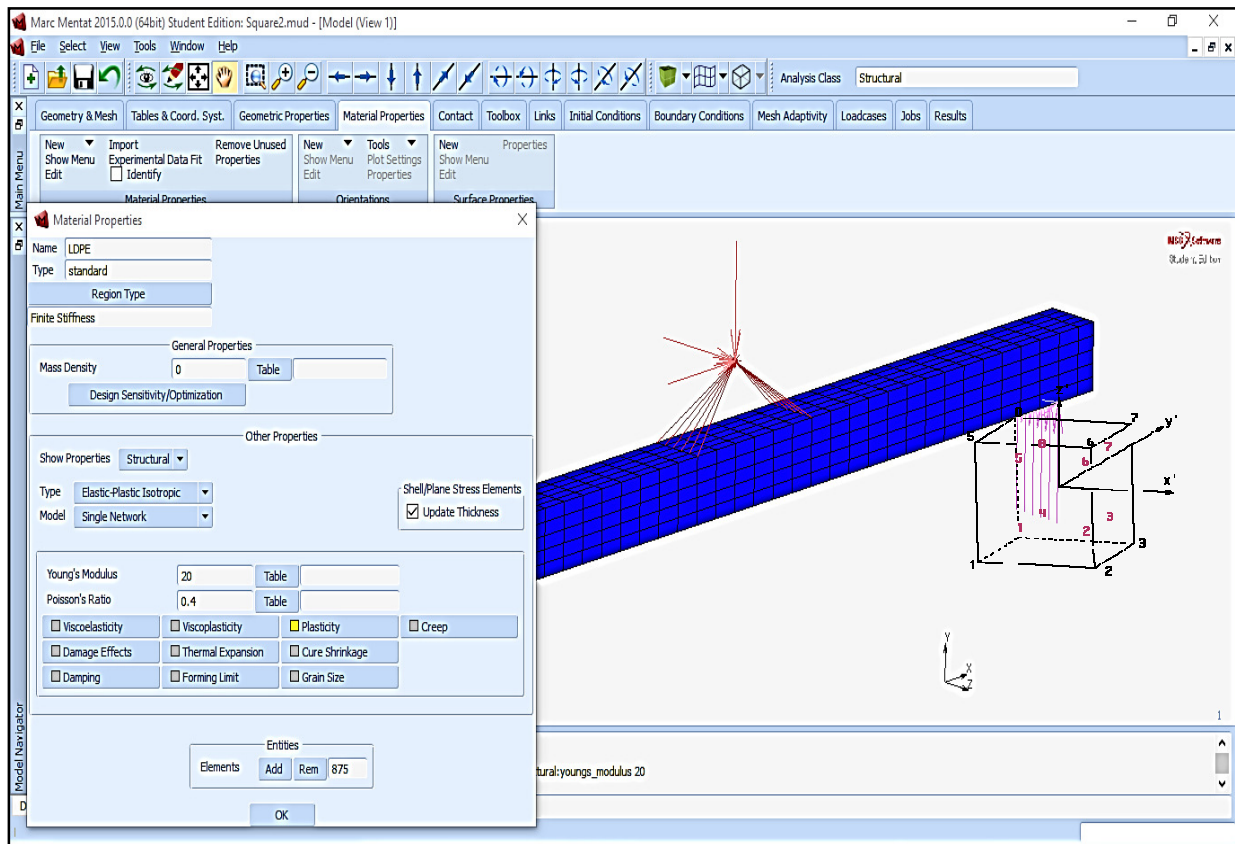
Figure (3.22): Defining LDPE material properties

45
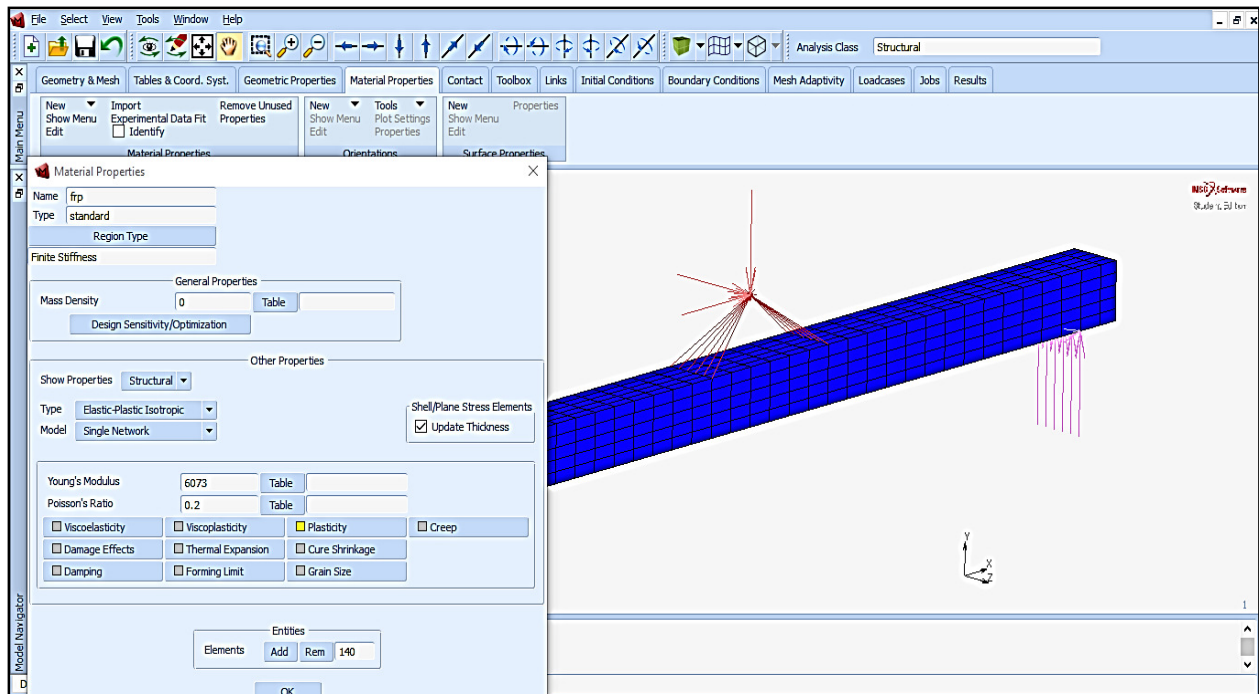
Figure (3.23): Defining FRP rebar material properties
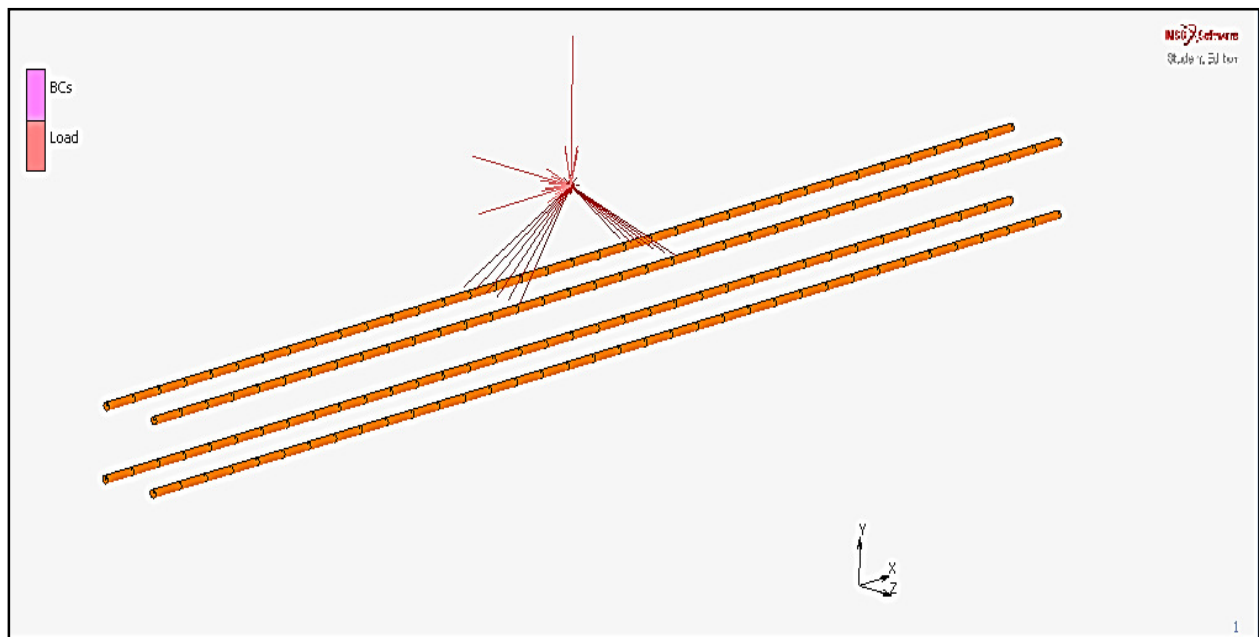
Figure (3.24): 3-D view of FRP rebars embedded in the LDPE Beam

Meshing helps in creating accurate results and to recreate the contour bands of Reaction Forces in Y-direction, stresses and strains, and displacements. The accuracy of finite

46

element modeling depends on the appropriate selection of boundary conditions (BC's) for which in our case is supported at the bottom and at the clear span of 150.75" (4.39 m).The BC's can be defined at the elemental mesh nodes and keeping them as pinned in our project. An example section of FRP rebar meshing has been shown in Figure (3.25).

A four-point loading regime is applied as shown in Figure (3.26). A reference point is taken in air outside the model and two node regions are selected and tied together to the reference point for the equal distribution of the applied load. A static load is applied at the reference point outside the model and is equally distributed between the points on the surface of the hybrid beam (Figure 3.27). In this experiment, the distance between the applied loads on the surface of the model is 32.5" (82.55 cm). Each step has an increment of 5 and maximum number of steps was set high in order to obtain the results before the complete failure state of the model.
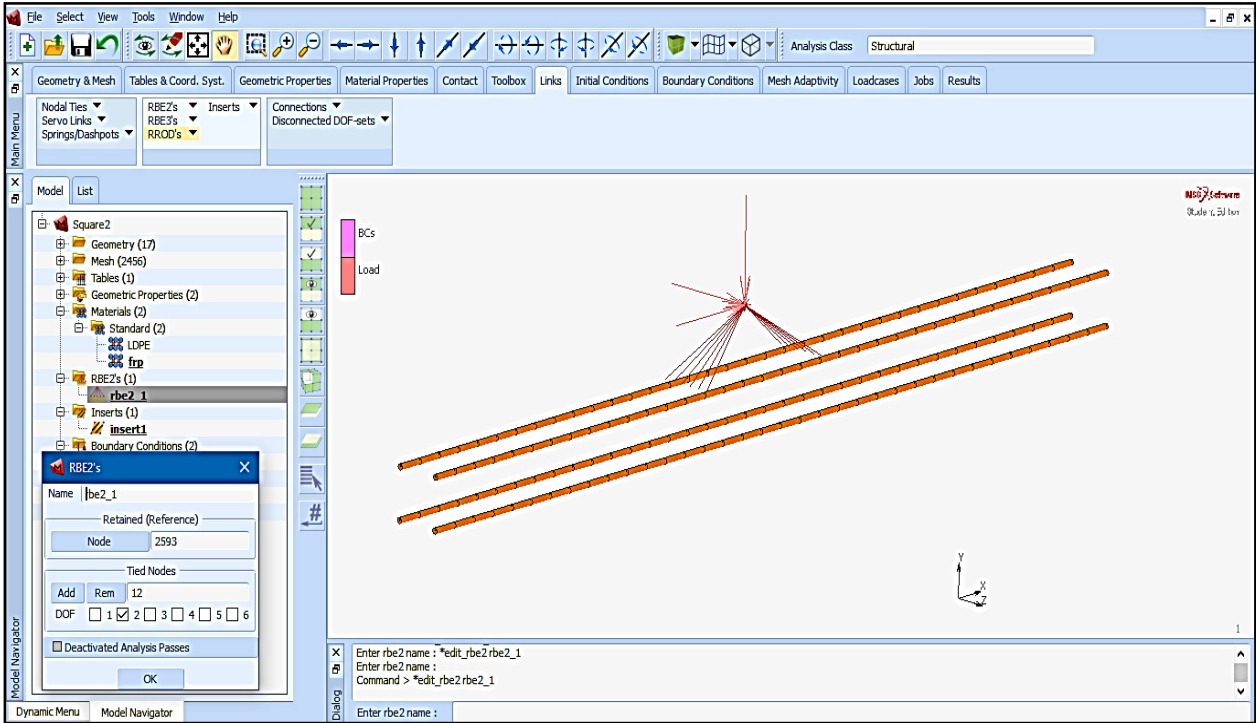
Figure (3.25): Rigid Links for application of the load on two points using a master node as reference
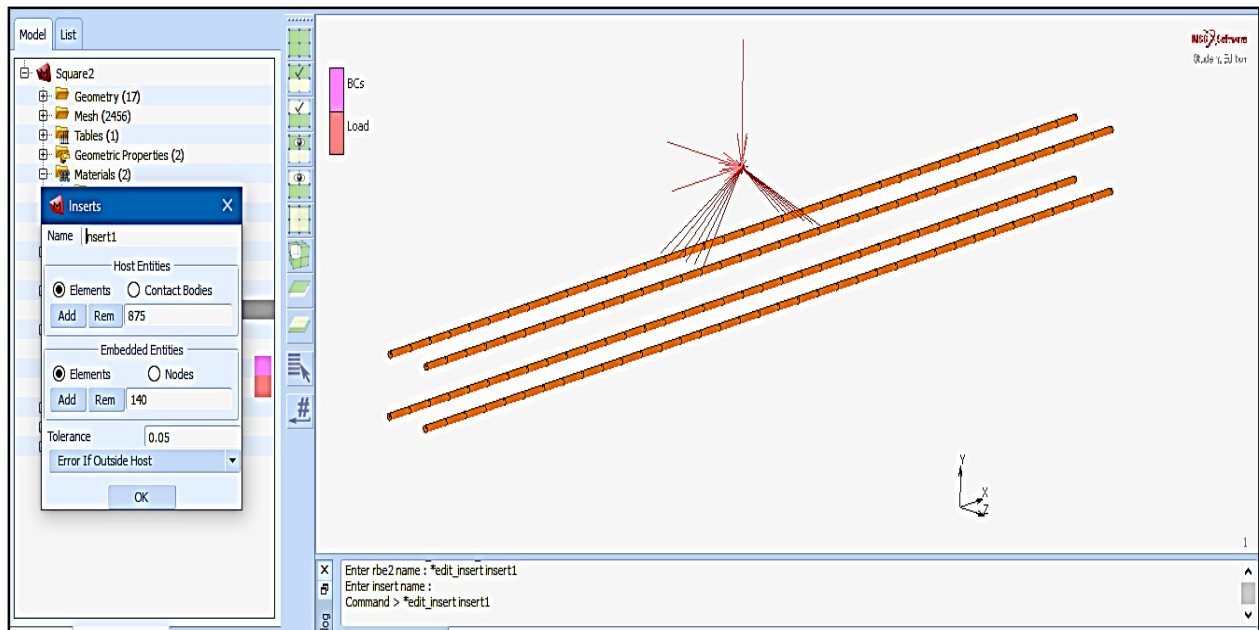
Figure (3.26): Using the insert tool for embedding the FRP rebars in the LDPE beam
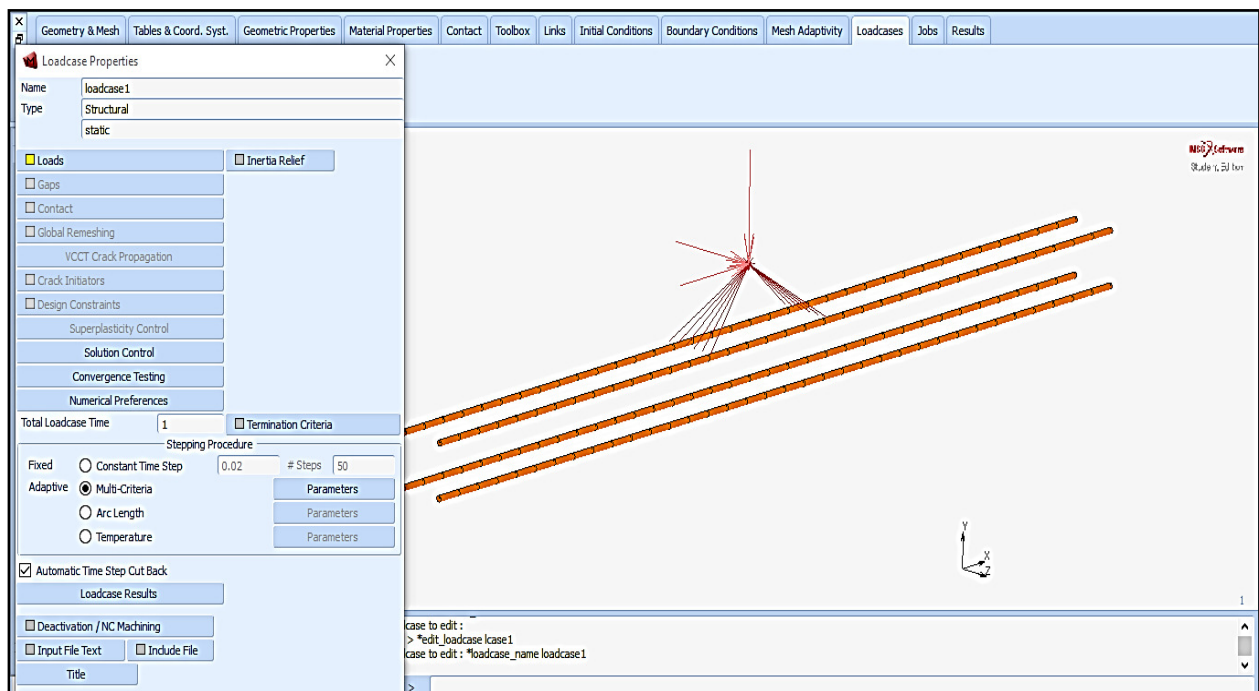
Figure (3.27): Define a static load case for simulation

Initially, the numerical analysis of the hybrid beam was linear up to a certain point, after which the nonlinearity is initiated. As expected, the nonlinear analysis is complex and hence it takes more time for the model to run.

Different set of results are obtained from the finite element analysis and are interpreted and compared with the experimental analysis and the graphs obtained.

3.5.4 ANALYSIS AND RESULTS OF BEAM SPECIMEN PPI-B408& PPI-B468 IN FINITE ELEMENT MODEL

The analysis of hybrid LDPE beam is run in Marc FE and the results are depicted as shown below. The load is applied to the model at 16.25" (41.28cm) from center on both the sides, illustrated in the Figure (3.21). The displacement in LDPE and embedded FRP rebar is shown in Figure (3.28 & 3.29) below. As similar to experimental results, the displacement is minimum/near to zero at the ends and maximum at the center. The displacement contour bands are depicted and maximum displacement is shown in blue contour band. Also the exact amount of displacement in FRP rebars is shown in Figure (3.29). It is evident that in the structural element, FRP rebars at the top is in compression and FRP rebars at the bottom are in tension. However, during the experiment, the slippage of FRP rebars indicates the improper bondage of the FRP rebars with the LDPE solid beam section. Hence, the top rebars tend to slip instead of going into compression completely. This was rectified in our finite element model by preventing the slippage and making the model stronger and displacing it less than the experiment values. The PPI-B468 and PPI-B408 simulated deflected shapes from finite element models have been shown in Figures (3.28through 3.31).
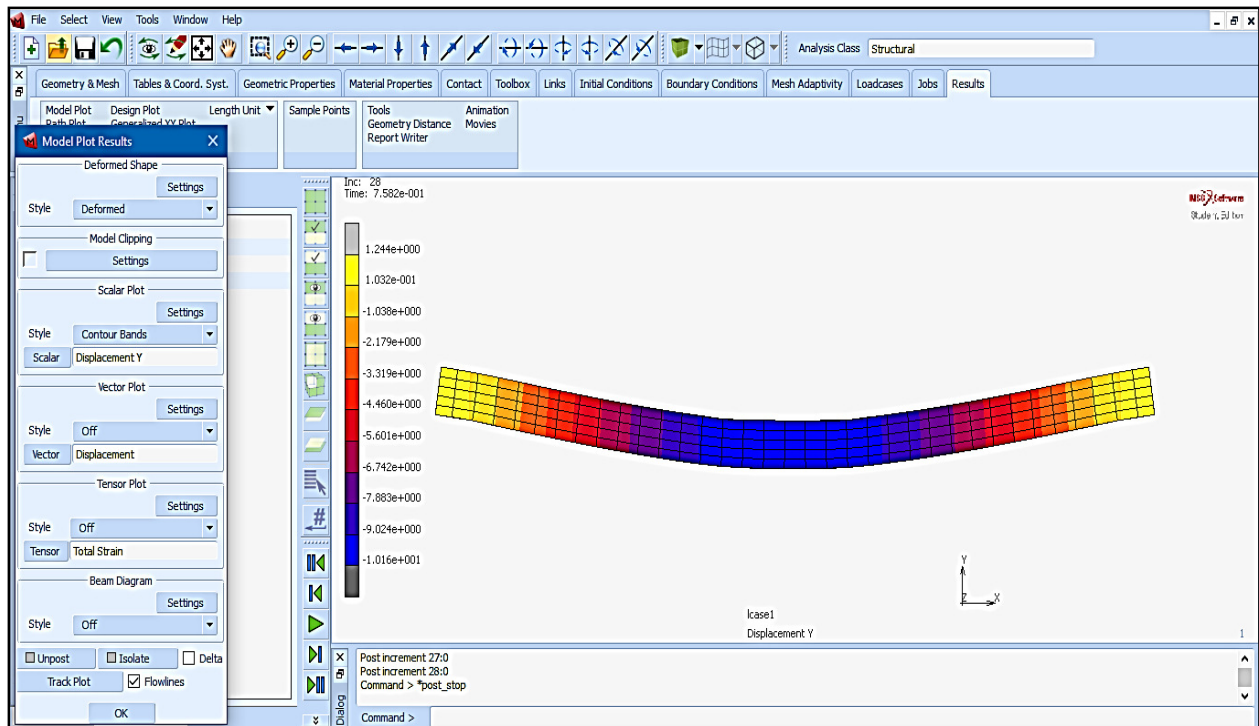
Figure (3.28): Exaggerated numerically-simulated deflected shape of the beam specimen PPI-B408
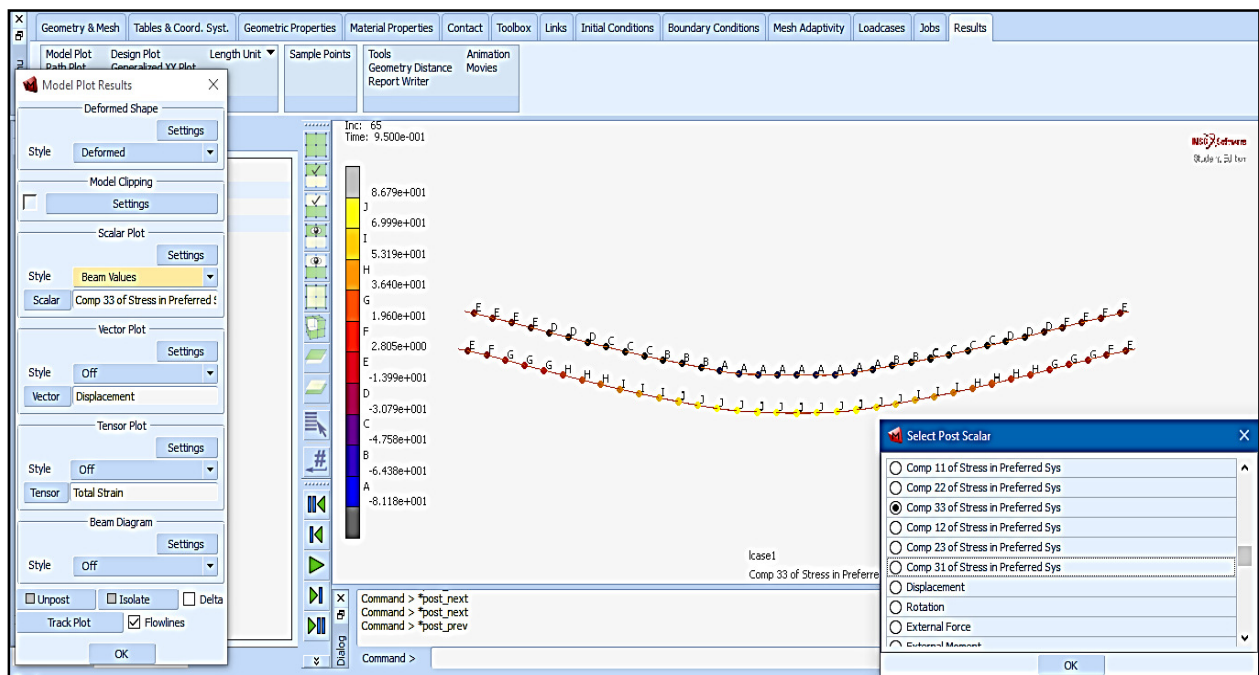
Figure (3.29): Exaggerated numerically-simulated deflected shape of FRP rebar yielding for beam specimen PPI-B408
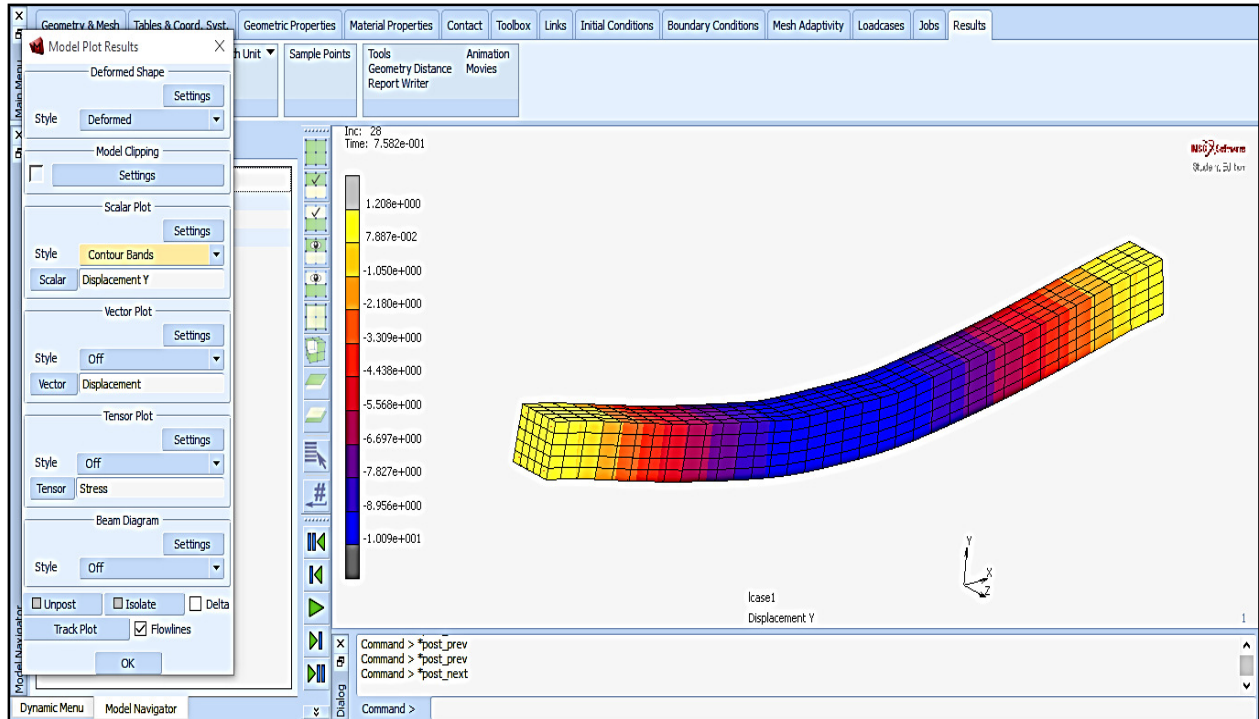
Figure (3.30): Exaggerated numerically-simulated deflected shape of the beam specimen PPI-B468
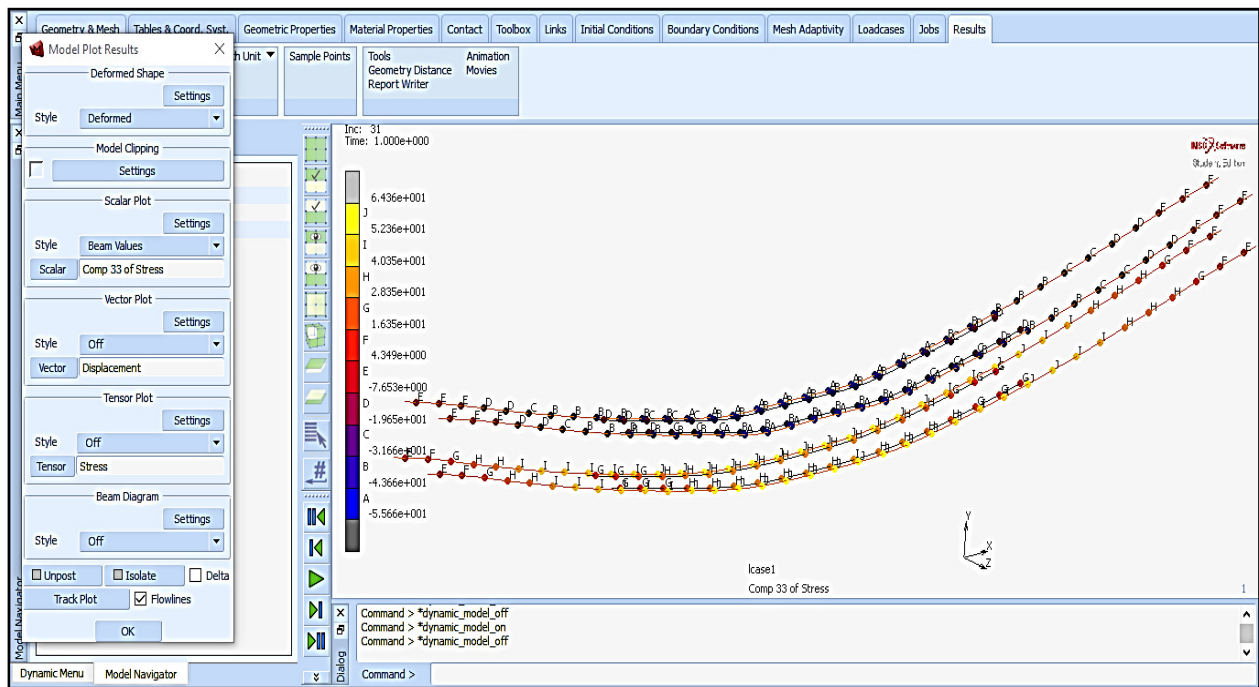
Figure (3.31): Exaggerated numerically-simulated deflected shape of FRP rebar yielding of beam specimen PPI-B468

A graphical representation of comparison between experimental results and finite element results has been depicted in the Figures(3.32 and 3.33).The experimental values are comparatively less due to the slippage of the FRP rebars which in turn causes loss of stress and more deflection in the beam at less static load.

From the comparison, it is evident that the higher yield stress values are because the finite element model is designed neglecting the slippage of FRP rebars embedded in the solid beam section. The analytical results are similar to the experimental results indicating the precise experimental procedure has been executed (Table 3.6). Similarly other types of hybrid LDPE beams can be directly modeled in MARC-MENTAT®and reliable results can be obtained from FE models.
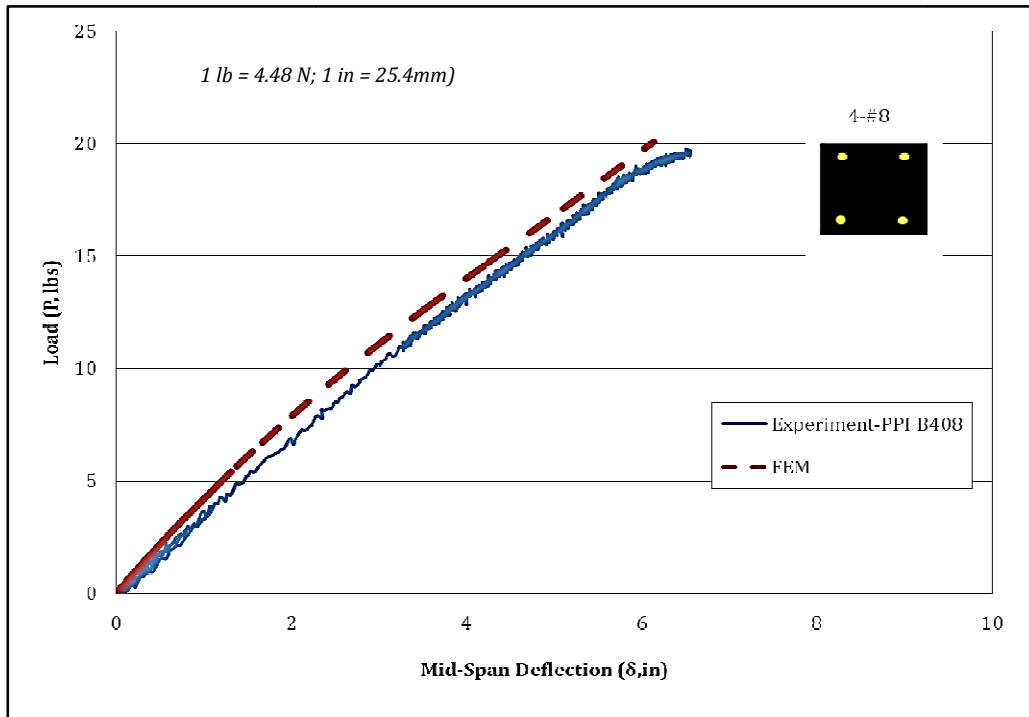
Figure (3.32): Load vs. Deflection comparison for PPI-B408 of Experimental and Finite element analysis
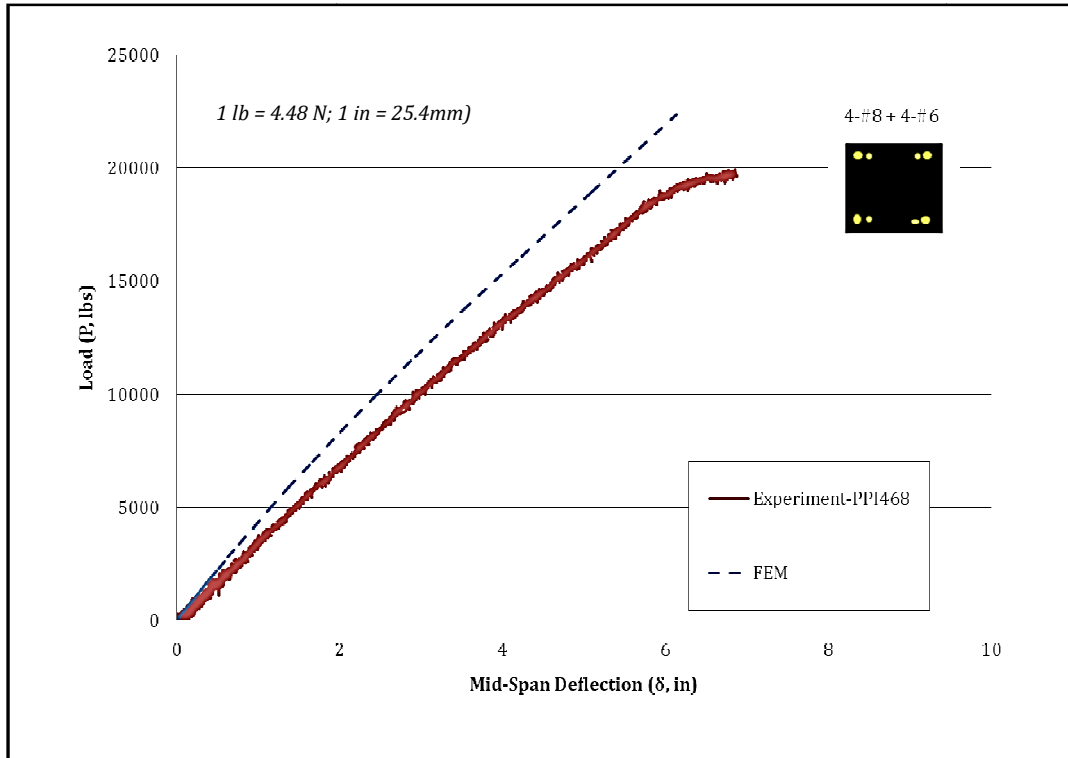
Figure (3.33): Load vs. Deflection comparison for PPI-B468 of Experimental and Finite element analysis

Table (3.6): Comparison between Theoretical and Experimental Stress Results

	Experimental kips[kN]	Analytical kips[kN]	FEM kips[kN]
PPI-B408	18 [80]	17.8 [79.2]	22 [97.9]
PPI-B468	20 [89]	21.3 [94.7]	24 [106.8]

3.4.5. DESIGN OF VARIOUS SIMILAR MODELS IN MARC MENTAT FOR FUTURISTIC ANALYSIS AND SCOPE

A total of nine FEmodels of the hybrid LDPE beams weredeveloped andanalyzed inMARC-MENTAT software. Beam models with different cross-sections and the number of rebars were evaluated. The results of the nine different FE models were then compared with each other. Graphs were plotted so as to investigate the substantial cross-sectional element

which can be used out in the field for better results and serviceability. This modeling provided a better understanding of the behavior of the composite members.

Three reinforcement details were analyzed and they are described Table(3.7). The three reinforcement details are:

1) One rebar #8 (1″ [25.4mm] diameter) at the center
2) Four rebars #8 (1″ [25.4mm] diameter) at the corners with 0.75" (19.05mm) cover
3) Four rebars #8 (1″ [25.4mm] diameter) + Four rebars #6 (0.75″ [19.05mm] diameter) positioned at the beam's corners with a plastic coverof 1.0″ (25.4mm).

Figures (3.34) through (3.36) present the results of a parametric study that was performed on the different finite element models. The dimensions of the square cross section of the beams are 10.0" X 10.0" X 17.0" (25.4cmX25.4cm X439.42cm) (width X depth X length), while for the rectangle cross section, the dimensions are 10.0″ X 15.0″X 173.0″ (25.4cm X 38.1cm X 439.42cm) and circle of diameter 10.0" (25.4cm). The cross section of the beam, number and location of the rebars are the major deciding factor in the flexural stiffness of the LDPE Hybrid beam. There is a huge difference with the load carried by different cross section and varying number of rebars. For example from the finite element results, it can be concluded that there is a significant jump of <u>174%</u> in the load carrying capacity from Square 401 to Square 408, and <u>125%</u> jump from Square 408 to Square 468.

Table (3.7): Different models used for parametric study and comparison

Type	Square (10"x10") (25.4cmx25.4cm)	Rectangle (10"x15") (25.4cmx38.1cm)	Circle (10" dia.) (25.4cm dia.)
(401) 1- #8 rebar at the center			
(408) 4- #8 rebars at the corners with 0.75" (1.9cm) cover			
(468) 4- #8 rebars + 4- #6 rebars at the corners with 1" (2.54cm) cover			
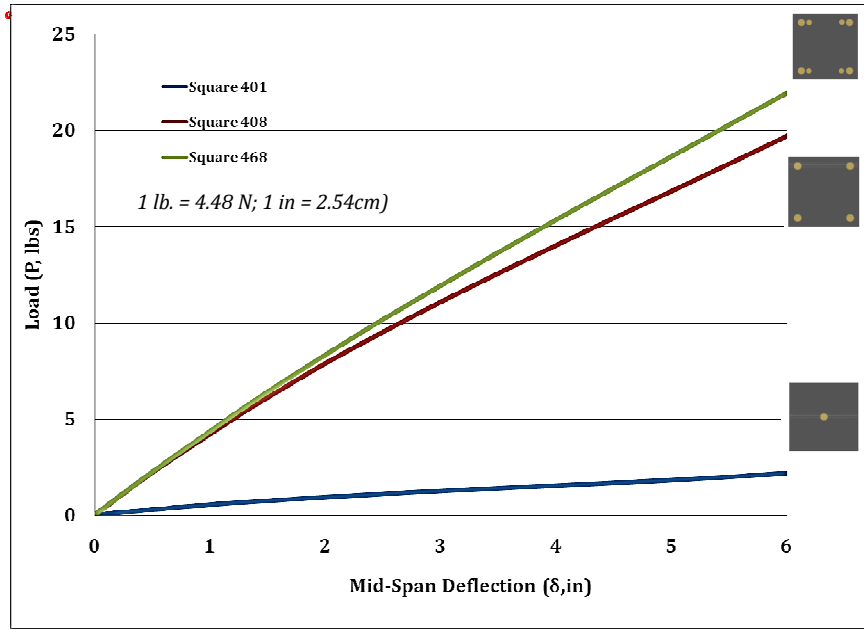
Figure (3.34): Comparison of square beam section with varying number of rebars
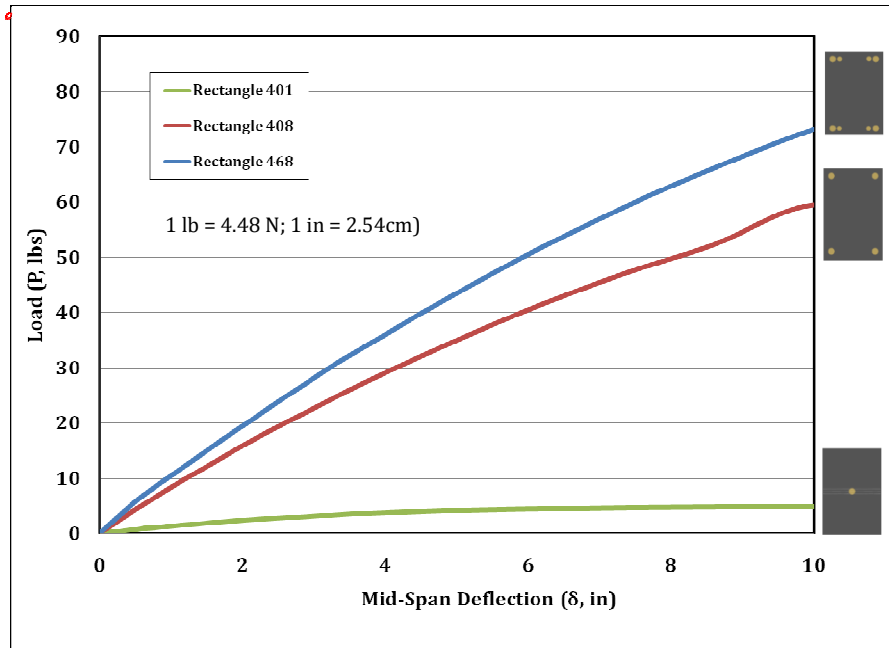
Figure (3.35): Comparison of Rectangle beam section with varying number of rebars
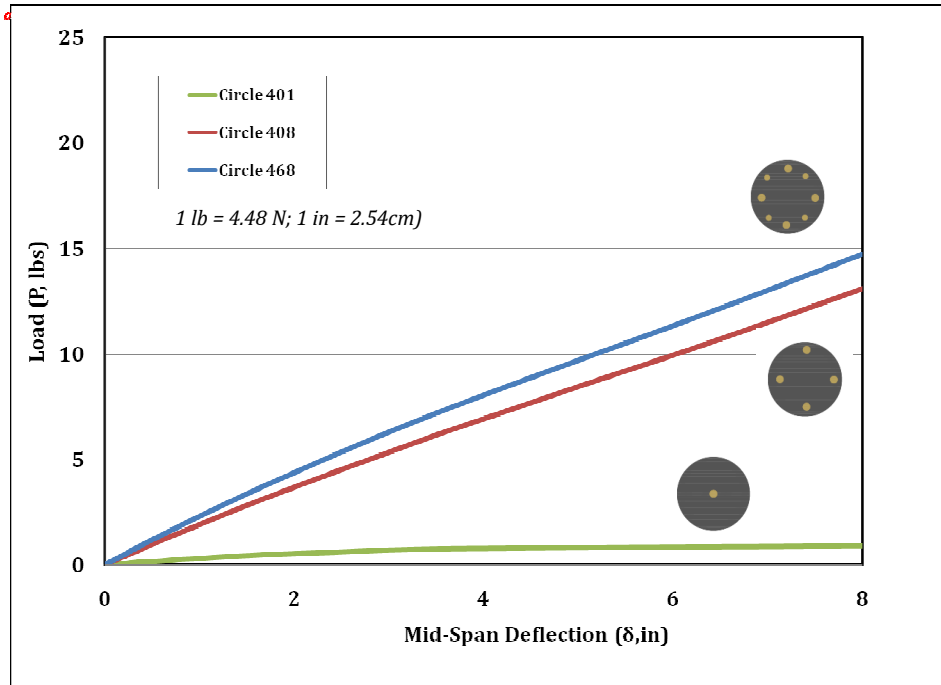
Figure (3.36): Comparison of circular beam section with varying number of rebars

Another comparison of the varying cross-sectional area of LDPE beam with the same number of rebars have been graphically compared (Figures 3.37 through 3.39) and is evident that the rectangular beam section can take more load than the other two cross-sections. This is due to the increased flexural stiffness of the rectangular beam is more than flexural stiffness of the square or circular bema section. Also there is a huge difference in the load carrying capacity with the difference in the location and number of rebars.

Lastly, a total load carrying capacity of the beam section and also the number of rebars has been graphically compared in the bar chart shown in Figures(3.40) and (3.41).
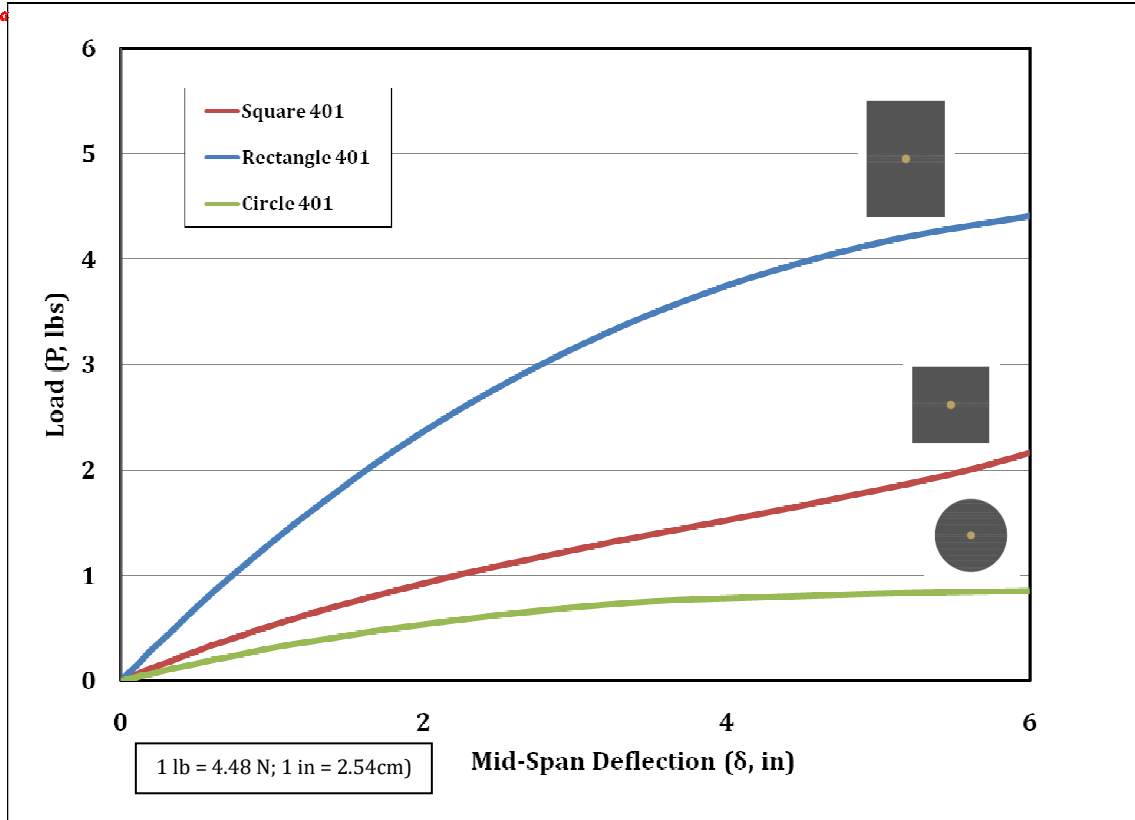
Figure (3.37): Comparison of different beam section with *one* rebar at the center
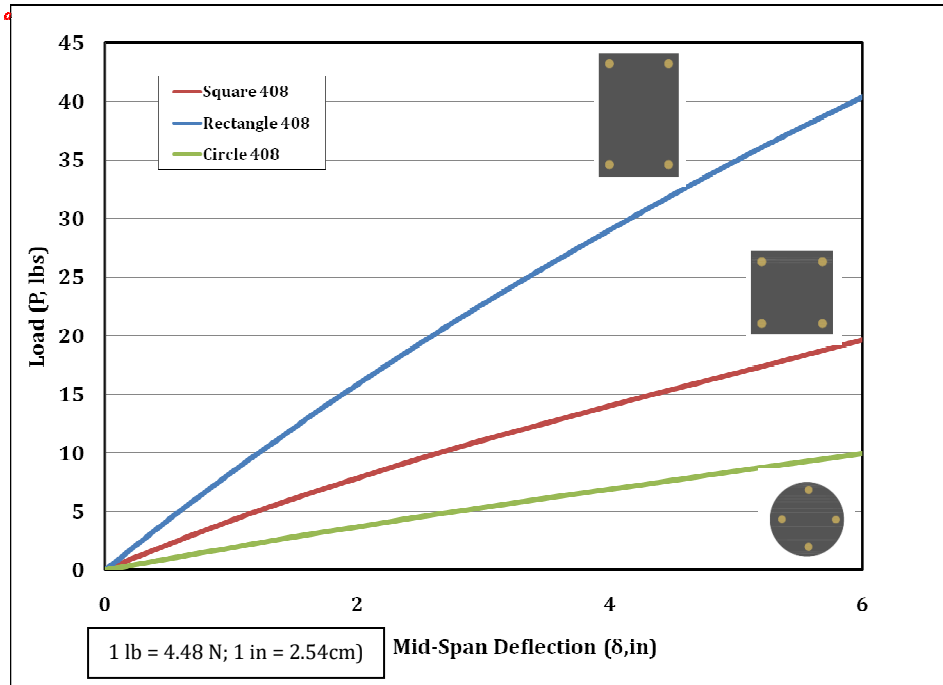
Figure (3.38): Comparison of different beam section with *four* rebars at the corner with a cover of 0.75" (19.05mm)
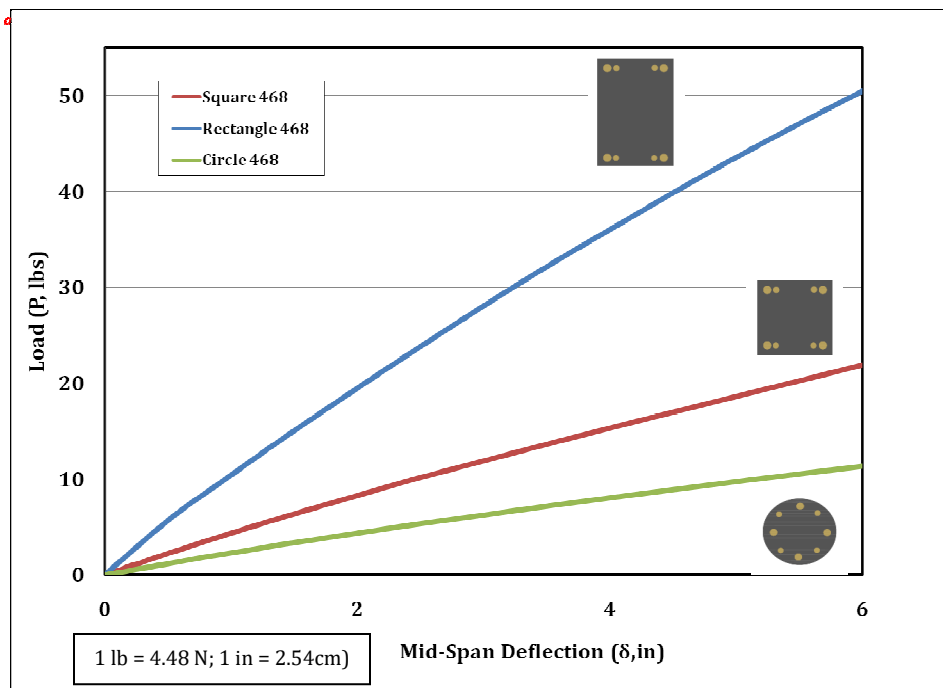
Figure (3.39): Comparison of different beam section with *eight* rebars at the corner with a cover of 1.0" (25.4mm)

Yield Stresses (in ksi)

1 lb = 4.448 N

	Circle	Square	Rectangle
401	1	5	8.5
408	12.5	20	59
468	15	25	75
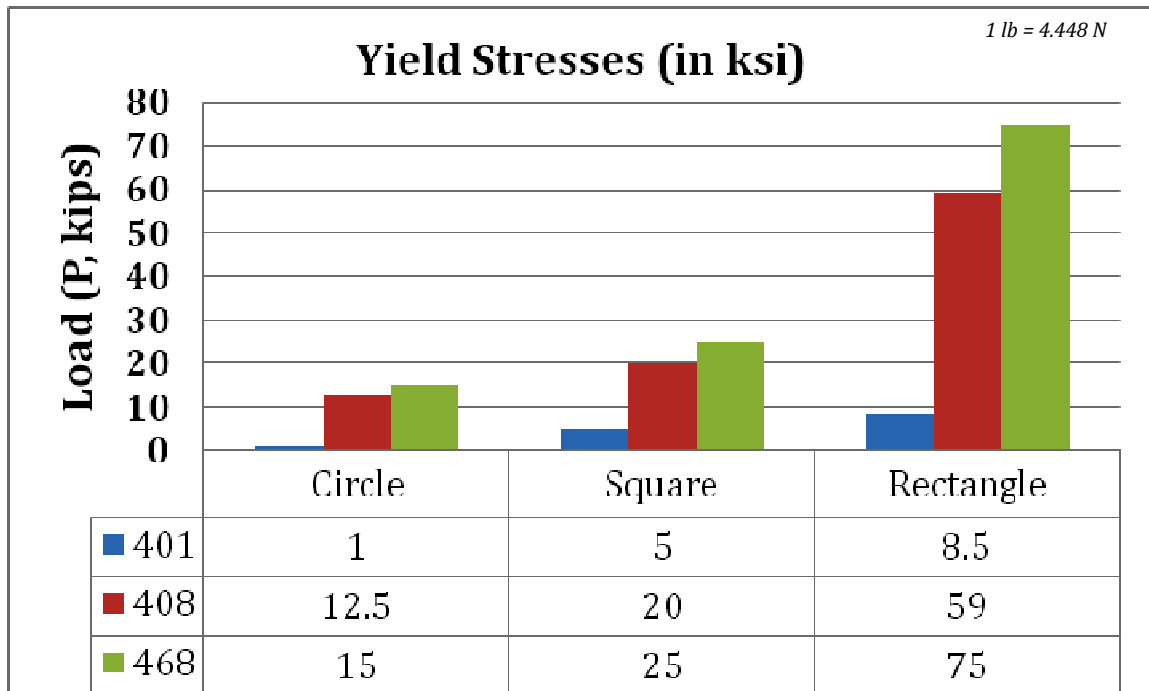
Figure (3.40): Comparison of different beam sections with varying number of rebars

Yield Stresses (in ksi)

1 lb = 4.448 N
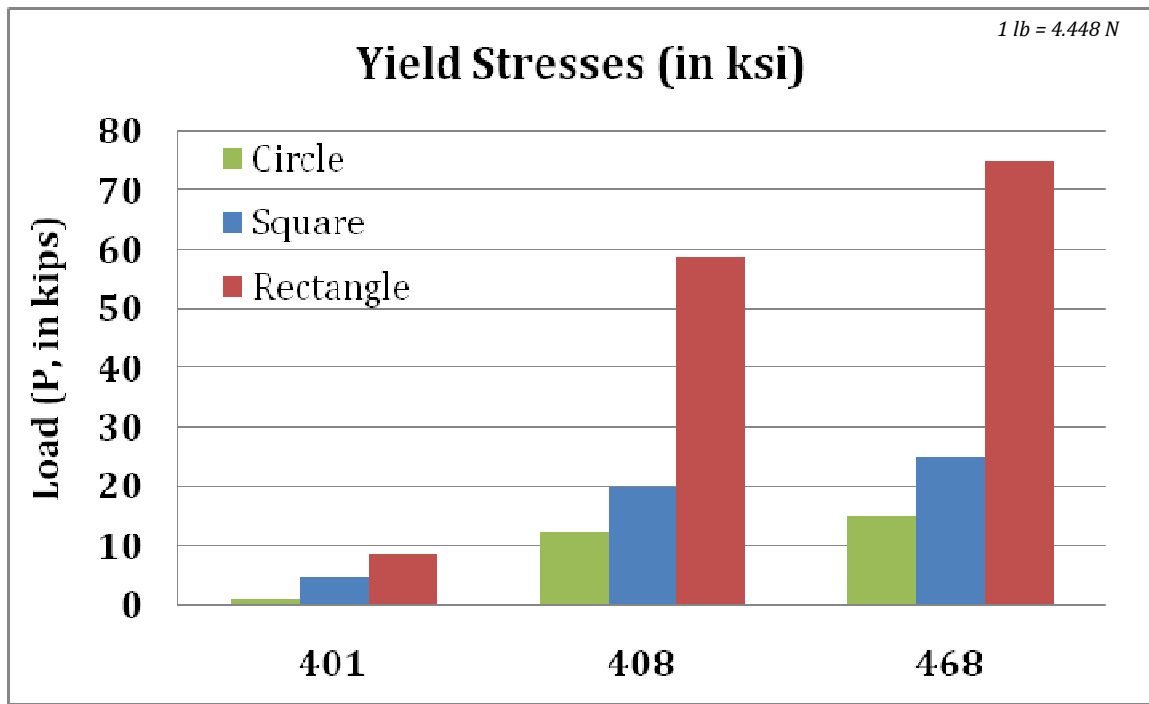
Figure (3.41): Comparison of different beam sections with varying number of rebars

60

CHAPTER 4

CONCLUSIONS AND RECOMMENDATIONS FOR FUTURE RESAERCH

4.1 General

This chapter presents a summary for the conclusions and recommendations for future research based on the outcomes of this study.

4.2 Conclusions

Based on the results of this study, the following conclusions are drawn:

♦ The hybrid beams evaluated in this program have met the target flexural stiffness of 0.276×10^6 kip-in^2 (1.9×10^6 MPa) at load levels of 25% and 50% of the yield stress. However, for specimen PPI-B408, the conservative value that was calculated at a higher load level approaching the non-linear range was slightly less (1.88%) than the target value (0.2708×10^6 kip-in^2 vs. 0.276×10^6 kip-in^2) (1.86×10^6 MPa vs. 1.9×10^6). As mentioned earlier, and due to the lack of ASTM or Caltrans procedures to calculate the stiffness, it the author's recommendations to use the linear value up to 50% of the yield stress for realistic prediction of the behavior of these hybrid systems. The use of the flexural stiffness at the recommended load level is the realistic and applicable value for conducting linear design of such hybrid beams, otherwise, a more sophisticated non-linear analysis that considered both the geometrical and materials nonlinearity will be required. However, it is believed that for this particular application a linear design based on EI calculated at a load level of about 50% of the yield load (beginning of the plastic range) is satisfactory for Caltrans bridge application,

♦ The beams exhibited a ductile behavior up to the maximum plastic load without the development of matrix cracks. This finding is very beneficial which indicates that the rebars, whether metallic or nonmetallic will be protected against moisture due to the integrated LDPE matrix up to the maximum load. It should be noted, however, although

61

FRP rebars do not rust, they may corrode when exposed to a wet environment if not protected. Test results provided evidence that the migration of moisture through matrix cracks has minimum impact on the durability of the internal FRP reinforcements. However, it is highly recommend that the exposed ends of the FRP rebars at the beams' ends be sealed with a compatible epoxy,

♦ The PPI hybrid beam specimens tested in this program have shown appreciable capabilities for absorbing energy which is crucial for this particular bridge protection application,

♦ The LDPE hybrid beams showed outstanding deformational capacities maintaining the ultimate moment resistance till the final stages of loading which indicate the tremendous ductility of this hybrid system,

♦ The simple theoretical model that has been developed to estimate the flexural capacity of the LDPE hybrid system is in line with the experimental results and it can effectively predict the ultimate moment with a negligible tolerance of 10 % of the actual flexural capacity,

♦ The theoretical approach of the experimental flexural capacity of the LDPE system involved the derivation of new equivalent rectangular stress blocks' parameters for both compression and tension zones with the values of $\beta_c = 0.82$, $\lambda_c = 0.79$, for compression and $\beta_t = 1.00$, $\lambda_t = 0.857$ for tension. These values can be used successfully, with a slightly conservative perspective, for any future design guidelines to estimate the flexural capacity of LDPE hybrid systems,

♦ The finite element does not simulate the slippage of FRP Rebars, hence it cannot capture the plastic behavior of the Hybrid LDPE beam,

♦ A broad conclusion can be made based on the cross-sectional area of solid beam and also the number and locations of rebars embedded in the LDPE beam. As the cross-section of the beam specimen increases, the flexural stiffness also increases resulting in higher load carrying capacity,

♦ In other words, a rectangular hybrid LDPE beam can take more load than a square or circular beam section with same number of rebars. 50% increase in the depth, increases the yielding strength of the LDPE beam by approximately 300% while having the FRP reinforcement at the corners (refer to Figure 3.38).

♦ The number and locations of rebars greatly influence the capacity of the beams. As simulated, a beam with one rebar at the center cannot take more load because the rebar is near to the neutral axis and hence does not contribute much to the capacity.

4.2 Recommendations for Future Research

Based on the results and the scope of this study, the following areas of research have been identified:

♦ In-depth investigation on the slippage of FRP rebars from the LDPE failure mode is needed,

♦ Further studies on the durability of the LDPE hybrid system are needed. This should include the creep behavior of the system,

♦ Fire behavior of this system also needs to be studied and the performance of the system under higher temperature needs further investigation,

♦ The evaluation of the system with different types of reinforcements such as steel, carbon/epoxy composites rebars and plates is also important to explore, and

♦ The slip behavior of the reinforcement due to mechanical mismatch needs more experimental and theoretical investigations.

REFERENCES

1) Mosallam A. S.,*(2005).“Large-Scale Experimental Evaluation of PPI Composite Beams”*, University of California, Irvine, Final Report, June 2005.

2) Mosallam A. S. (*2006). “Out-Of-Plane Flexural Behavior of Unreinforced Red Brick Walls Strengthened with FRP Composites,”* Composites Part B: Engineering Volume 38, Issues 5–6, July–September 2007, pp. 559–574.

3) Stroke F. E., (2002), “*Axial Compression Test on Plastic Piles”*, Lehigh University, Test Report, Lehigh University, Lehigh, PA, August.

4) Laursen, P. T., Seible F., Hegemier G.A., *(*1995).“*Seismic Retrofit and repair of Reinforced Concrete with Carbon Overlays,*” Report No. SSRP-95101, University of California, San Diego, USA..

5) Tantayanondkul C., (2006), *“Experimental Compression and Tension Stress-Strain Relations for LDPE Materials”,* University of California, Irvine, Research Report.

6) Ferguson P., Breen J., and Jirsa J., *“Reinforced Concrete Fundamentals*”, 5th Ed., Wiley, 1988.

7) Asaro R. J., (2000), “Three Point Bend Test of Plastic Pilings Hybrid HDPE-LDPE/Steel Pipe”, Test Report, June 2000.

8) Lu G., (2002), “*HDPE Wood-Plastic Composite Materials Model Subjectto Damage”,* M.Sc. Thesis, Civil and Environmental Engineering Department, Washington State University, Pullman, WA, USA.

9) Cowin S. C., and M. M.Mehrabadi(1992). “*The Structure of the Linear AnisotropicElastic Symmetries”,* Journal of Mech. Phys. Solids, 40.7, 1459-1471.

10) Zhu Y. and S.Cescotto(1995) “*A Fully Coupled Elastic-Visco-Plastic Damage Theory for Anisotropic Materials”*, International Journal of Solids and Structures, 32,11, 1607-1641.

11) Haiar K. J., (2000), *"Performance and Design of Prototype Wood-Plastic Composite Sections"*, Thesis for partial fulfillment of the degree of Master of Science, Washington State University, Pullman, WA, USA.

12) ASTM D 638 (1994; Rev. B), *"Tensile Properties of Plastics"*, American Society for Testing and Materials, Philadelphia, PA, USA.

13) ASTM D 695 (1991). *"Compressive Properties of Rigid Plastics",* American Society for Testing and Materials, Philadelphia, PA

14) Plastics Pipe Institute, *"Engineering Properties of Polyethylene"*, Handbook of Polyethylene Piping, http://plasticpipe.org/publications/pe-handbook.html (*free download*).

15) Hoechst Celanese Corporation (1989), "Designing with Plastic - The Fundamentals", Engineering Plastics Division Chatham, NJ.

16) Yanyan Sha, Hong Hao, (2012), "*Nonlinear finite element analysis of barge collision with a single bridge pier*", School of Civil and Resource Engineering, The University of Western Australia, WA, Australia.

17) Mosallam A. S., Bayraktar A., Elmikawi M., Pul S., Adanur S., (2014), "*Polymer Composites in Construction: An Overview",* University of California, Irvine.

18) Malvar L. J., (1995), *"Tensile and Bond Properties of GFRP rebars",* University of California, Davis.

This appendix presents the actual stiffness values of the two beam specimens. The results of this analysis indicated that both beams have met the target flexural value of 0.27 X 109 lb-in^2.

A. BEAM SPECIMEN PPI-B468

A.1 CALCULATION OF SECTION'S FLEXURAL STIFFNESS
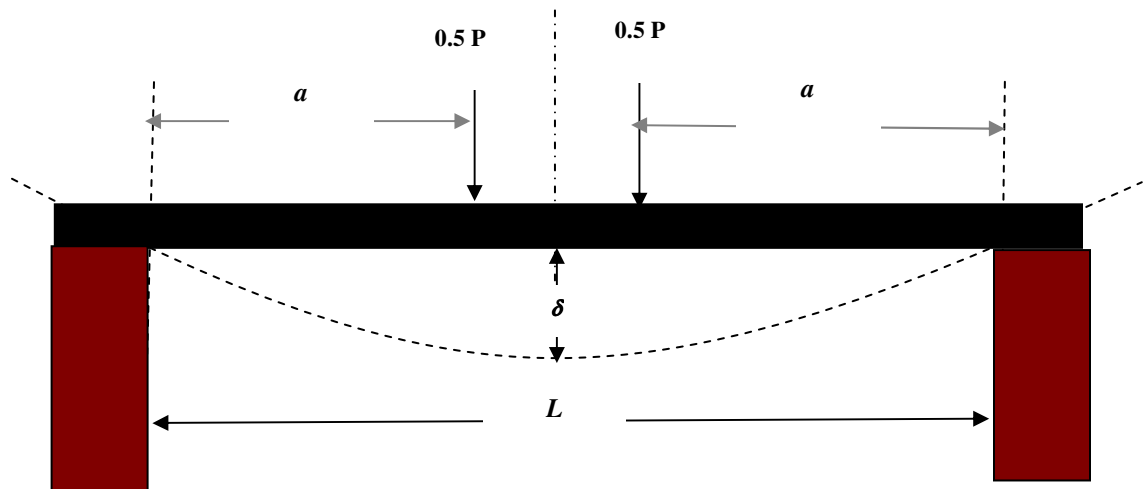
Figure (A.1): Elastic Line & Loading

For 4-point simply supported loaded beam (Figure A.1), the flexural deflection is given by:

$$\delta_{center} = \frac{Pa}{48EI_{eff}}\left(3L^2 - 4a^2\right) \qquad (1.1)$$

From which

$$EI = D = \frac{a}{48}\frac{P}{\delta}\left(3L^2 - 4a^2\right) \qquad (1.2)$$

where:

δ = Central deflection at the end of the elastic linear range (refer to Figure (6))

D = Section Flexural stiffness (EI), lb-in^2 (kN-m^2)

a = Distance from the support to the point load = 59.5" (1.51 meters), and

L = Clear Span = 150.75" (3.83 meters)

A.1.1 Low-Stress Linear Range (5-kip[22.24 kN] Loading Level)

The average slope value of the linear portion up to a load level of 5 kips extracted from the experimental P/δ curve shown in Figure (3.8) is found to be:

$$\frac{P}{\delta} = 5,405.41 \ lb/in \ (946.6 \ MPa)$$

Thus, the flexural stiffness at this load level can be calculated using Eqn. (1.2) as follows:

$$EI^{5kip} = D = \frac{59.5"}{48}(5,405.41\frac{lb}{in})(3(151.5")^2 - 4(59.5")^2) = 0.366X10^9 \ lb - in^2 (2.5X10^6 \ MPa)$$

A.1.1 Medium-Stress Linear Range (10-kip[44.48 kN]Loading Level)

The average slope value of the linear portion up to a load level of 10 kips extracted from the experimental P/δ curve shown in Figure (3.9) is found to be:

$$\frac{P}{\delta} = 4,675.08 \ lb/in \ (818.7 \ MPa)$$

Substituting by this value in Eqn (1.2), gives:

$$EI = D = \frac{59.5"}{48}(4,675.08\frac{lb}{in})(3(151.5")^2 - 4(59.5")^2) = 0.317X10^9 \ lb - in^2 (2.18X10^6 \ MPa)$$

A.1.1 Near-Yield Linear Range (21,359kip [95.0 kN]Loading Level)

The average slope value of the near-linear portion up to a yield load level extracted from the experimental P/δ curve shown in Figure

$$\frac{P}{\delta} = 4,297 \ lb/in \ (752.5MPa)$$ (3.7) is found to be:

Substituting by this value in Eqn. (1.2), gives:

$$EI = D = \frac{59.5"}{48}(4,297\frac{lb}{in})(3(151.5")^2 - 4(59.5")^2) = 0.291X10^9 \ lb - in^2 (2.0MPa)$$

A.2 CALCULATION OF MAXIMUM LINEAR AND ULTIMATE PLASTIC MOMENT CAPACITIES

888

A.2.1 Maximum Linear Moment Capacity:

Based on full-scale test results, the maximum linear moment capacity (refer to Figure (6)) is:

$$M_{Max}^{Linear} = \frac{21,415.5 lbs}{2} 59.5" = 637,111.13 lb - in = 637\, kip - in = 53.1 kip - ft\, (71.9 kN - m)$$

A.2.2 Maximum Plastic Moment Capacity:

This value is calculated using the ultimate peak load in the plastic range. As shown in Figure (6), the maximum plastic load was 24,390.0lbs (108.0kN). Thus:

$$M_{Max}^{Plastic} = \frac{24,390\, lbs}{2} 59.5" = 725,602.5\, lb - in = 725.8\, kip - in = 60.47\, kips - ft\, (81.9 kN - m)$$

A.2.3 Maximum Flexural Stress:

Maximum flexural stress = 0.524 ksi (3.6 MPa) which is about 40% of the ultimate tensile strength of PPI-LDPE matrix material which is 1.325 ksi [9.13 MPa].

A summary of the results for specimen PPI-B468 is presented in Table (A.1).

B. BEAM SPECIMEN PPI-B408

B.1 CALCULATIONS OF SECTION'S FLEXURAL STIFFNESS

B.1.1 Low-Stress Linear Range (5-kip [22.24 kN] Loading Level)

The average slope value of the linear portion up to a load level of 5 kips extracted from the experimental P/δ curve shown in Figure (3.13) is found to be:

$$\frac{P}{\delta} = 4{,}166.70 \ lb/in (729.5 MPa)$$

Thus, the flexural stiffness at this load level can be calculated using Eqn. (1.2) as follows:

$$EI^{5kip} = D = \frac{59.5"}{48}(4{,}166.7\frac{lb}{in})\big(3(151.5")^2 - 4(59.5")^2\big) = 0.2828 X 10^9 \ lb-in^2 (1.9 X 10^6 MPa)$$

B.1.1 Medium-Stress Linear Range (10-kip [44.48 kN] Loading Level)

The average slope value of the linear portion up to a load level of 10 kips extracted from the experimental P/Δ curve shown in Figure (3.14) is found to be:

$$\frac{P}{\delta} = 4{,}132.64 \ lb/in (723.6 MPa)$$

Substituting by this value in Eqn (1.2), gives:

$$EI = D = \frac{59.5"}{48}(4{,}132.64\frac{lb}{in})\big(3(151.5")^2 - 4(59.5")^2\big) = 0.2803 X 10^9 \ lb-in^2 (1.9 X 10^6 MPa)$$

B.1.1 Near-Yield Linear Range(17.81kips [79.22 kN] Loading Level)

The average slope value of the near-yield linear portion of the experimental P/δ curve shown in Figure (3.12) is found to be:

$$\frac{P}{\delta} = 4{,}000 \ lb/in (700.5 MPa)$$

Substituting by this value in Eqn. (1.2), gives:

$$EI = D = \frac{59.5"}{48}(4{,}000\frac{lb}{in})\big(3(151.5")^2 - 4(59.5")^2\big) = 0.2708 X 10^9 \ lb-in^2 (1.86 X 10^6)$$

B.2 CALCULATION OF MAXIMUM LINEAR AND ULTIMATE PLASTIC MOMENT CAPACITIES

B.2.1 Maximum Linear Moment Capacity:

Based on full-scale test results, the maximum linear moment capacity for specimen PPI-B408 is:

$$M_{Max}^{Linear} = \frac{17{,}957.8lbs}{2}59.5" = 534{,}244.6 lb - in = 534.24 kip - in = 44.53 kip - ft\,(60.37\,kN - m)$$

B.2.2 Maximum Plastic Moment Capacity:

This value is calculated using the ultimate peak load in the plastic range. The maximum plastic load was 24,371 lbs (108.4 kN). Thus

$$M_{Max}^{Plastic} = \frac{24{,}371\,lbs}{2}59.5" = 725{,}037.25\ lb - in = 725.04\ kip - in = 60.42\ kip - ft\,(81.9\,kN - m)$$

B.2.3 Maximum Flexural Stress:

Maximum flexural stress = 0.84 ksi(5.8 Mpa)(about 63.2% of the ultimate tensile strength of the LDPE material which is 1.325 ksi [9.1 MPa]).

A summary of the results for specimen PPI-B408 is presented in Table (A.1).

Table (A.1): Summary of Results

Beam Specimen	Load Level (kips) (kN)	*P/δ* Experimental Value (lb/in) (kN/m)	Linear Flexural Stiffness, (X 10⁹ lb-in²) (X10⁹kN/m²)	Yield Moment Capacity (kip-ft) (Nm)	Maximum Plastic Moment Capacity (kip-ft)
PPI-B468	5 (22.24)	5,405.41 (964.5)	0.3661 (2.52)	53.10 (72.0)	60.47 (81.98)
	10 (44.48	4,675.08 (818.7)	0.3171 (2.18)		
	Yield (21.35) (94.96)	4,297.06 (749.4)	0.2910 (2.0)		
PPI-B408	5 (22.24)	4,166.70 (729.7)	0.2828 (1.95)	44.53 (60.37)	60.42 (81.9)
	10 (44.48)	4,132.64 (723.7)	0.2803(1.93)		
	Yield (17.8) (79.1)	4,000 (700.5)	0.2708 (1.86)		